Available online at www.sciencedirect.com
ScienceDirect
Comput. Methods Appl. Mech. Engrg. 196 (2007) 3624–3649
Computer methods in applied mechanics and engineering
www.elsevier.com/locate/cma

Numerical methods for extracting edge stress intensity functions in anisotropic three-dimensional domains

Zohar Yosibash *, Netta Omer

Pearlstone Center for Aeronautical Engineering Studies, Department of Mechanical Engineering, Ben-Gurion University of the Negev, 84105 Beer-Sheva, Israel

Received 1 November 2005; accepted 30 October 2006
Available online 12 March 2007

Dedicated to Prof. Ivo Babuška on the occasion of his 80th birthday.

Abstract

The solution to elasticity problems in three-dimensional (3-D) polyhedral domains in the vicinity of an edge is represented by a family of eigen-functions (similar to 2-D domains) complemented by shadow-functions and their associated edge stress intensity functions (ESIFs), which are functions along the edge. These are of major engineering importance because failure theories directly or indirectly involve them.

In isotropic materials one may compute analytically the eigen-functions and their shadows [Z. Yosibash, N. Omer, M. Costabel, M. Dauge, Edge stress intensity functions in polyhedral domains and their extraction by a quasi-dual function method, Int. J. Fract. 136 (2005) 37–73], used in conjunction with the quasi-dual function method [M. Costabel, M. Dauge, Z. Yosibash, A quasi-dual function method for extracting edge stress intensity functions, SIAM J. Math. Anal. 35 (5) (2004) 1177–1202] for extracting ESIFs from finite element solutions. However, in anisotropic materials and multi-material interfaces the analytical derivation becomes intractable and numerical methods are mandatory. Herein we use *p*-finite element methods (*p*-FEM) for the computation of the eigen-pairs and shadow functions (together with their duals). Having computed these, the *p*-FEM is used again to obtain a FE solution from which we extract approximations of the ESIFs based on a family of adaptive hierarchical Jacobi polynomials of increasing order.

Numerical examples for 3-D isotropic and anisotropic materials are provided for which the eigen-pairs and shadow functions are numerically computed and ESIFs extracted. These examples show the efficiency and high accuracy of the numerical approximations.

Keywords: Edge stress intensity functions; *p*-FEM; Fracture mechanics

1. Introduction

Mechanical failures in anisotropic laminated composites and electronic devices are usually observed along edges. Therefore, an increasing interest in predicting and eventually preventing these failures leads to renewed interest in the solutions of three-dimensional linear elastic problems at edges. Due to the complex treatment of the elasticity system in the vicinity of a three-dimensional edge, most of the research in the past has focused on two-dimensional (2-D) domains under the assumption of plane stress or plane strain. The 2-D elastic solution in polygonal domains in the vicinity of reentrant corners, and especially crack tips, has been studied for over 50 years and known to be expressed as an asymptotic series. It is described in terms of special singular functions (eigen-functions) depending on the geometry and the boundary conditions in the vicinity

* Corresponding author. Tel.: +972 8 6477103; fax: +972 8 6477101.
E-mail addresses: zohary@bgu.ac.il (Z. Yosibash), nettao@bgu.ac.il (N. Omer).

0045-7825/$ - see front matter
doi:10.1016/j.cma.2006.10.017

of the corner on one hand, and of unknown coefficients (stress intensity factors) depending on the given body forces and tractions on the other hand. The eigen-pairs (eigen-values and eigen-functions) may be obtained by several techniques. An analytical method for computing eigen-pairs in isotropic domains is provided in many prior publications [21,12,9,2]. A semi-analytic approach for the eigen-pairs computations was presented in [6], applicable to anisotropic domains. Many numerical methods were developed, as for example in [13,20,23] which are applicable also to anisotropic and multi-material interfaces.

In daily basis applications of fracture mechanics, configurations which are inherently three-dimensional (3-D) are quite frequently encountered. In 3-D polyhedral domains, the solution is represented by three different asymptotic expansions based on its vicinity to either an edge, a vertex or a vertex-edge [8]. In the vicinity of *edges* the solution may be represented by a series expansion characterized by *exponents* α_i which belongs to a discrete set of eigen-values and that each eigen-value has an associated *eigen-function* $\boldsymbol{\varphi}_0^{(\alpha)}(\theta)$. These eigen-pairs depend only on the geometry, material properties and boundary conditions in the vicinity of the edge and may be computed by solving a set of 2-D problems. The coefficients of the series expansion are *functions* along the edge, denoted by $A_i(x_3)$ (x_3 is a coordinate along the edge). $A_i(x_3)$ is associated with the ith eigen-value and called "edge stress intensity function" (ESIF) which determines the "amount of energy" residing in each singularity. From the engineering perspective $A_i(x_3)$ associated with $\alpha_i < 1$ are of major importance because these are correlated to failure initiation. *In addition to the eigen-pairs*, "*new functions*" *appear in the series expansion in* 3-*D domains*, *called* "*shadows*", *that have no counterparts in* 2-*D domains*, *see* [7]. The edge eigen-pairs and their shadows in cracked or notched domains were first addressed by Hartranft and Sih in [10]. At the time however, these were not presented explicitly and the general structure of the asymptotic expansion not observed. Based on the abstract formulation in [7] we have expressed explicitly in [22] the series solution in the vicinity of an edge as a combination of eigen-functions and their shadows for *isotropic materials*. We provided the mathematical algorithm for the construction of the asymptotic elastic solution in the vicinity of an edge (which is an extension of the two-dimensional case), and a new extraction method named *quasi-dual function method*, was applied to obtain the polynomial approximation of the ESIFs. This method can be viewed as an extension of the dual function extraction method in 2-D [3,18] and its theoretical details were firstly introduced in [7]. Application of the quasi-dual function method for the extraction of EFIFs from finite element (FE) solution requires the dual eigen-functions and their dual shadows which may be computed analytically for isotropic domains.

In anisotropic and multi-material interfaces, the eigen-functions, their shadows and the dual eigen-functions cannot be computed analytically, and numerical methods are required. Because these functions are analytic and depend on one variable, the use of p-FEMs for their computation possess the advantage of exponential convergence rates. Using the numerically computed eigen-functions, their duals and shadows, the functional $J[R]$ is used [7,22] which is a surface integral along a cylindrical surface in order to compute the ESIF explicitly as a function of x_3 (the coordinate along the edge). The $J[R]$ computation is a post-processing step in a p-version finite element code. To demonstrate the accuracy and efficiency of ESIFs extraction two example problems are considered – a crack in an isotropic domain for which an analytical solution exists, and a crack in an anisotropic domain. This method *provides the functional representation of the ESIFs along* x_3, as opposed to other methods providing point-wise values of the ESIFs along the edge as the J-integral [11] and the H-integral [15]. Most importantly, *the method is adaptive*, providing a better polynomial representation of each of the ESIFs as the special hierarchical family of extraction polynomials is increased.

This paper is organized as follows:

- We start with notations, the linear anisotropic elastic problem and asymptotic expansion of the solution in the neighborhood of an edge in Section 2.
- The weak formulation for the computation of the primal eigen-pairs and their duals, followed by the p-FEM formulation are provided in Section 3.
- Using the primal eigen-pairs, we proceed to the weak formulation required for the computation of the shadow functions and their duals in Section 4.
- To demonstrate the accuracy and efficiency of the proposed numerical method for the computation of eigen-pairs, dual and shadow functions, we consider an isotropic domain for which the analytical solution is available. In Section 5 a cracked isotropic domain with traction free boundary conditions is considered. Comparison of the eigen-pairs, dual and shadow functions computed by p-FEMs with the analytical values show an exponential convergence rate. For this problem we provide in Appendix A the explicit analytic formulas for the eigen-functions, duals and shadows.
- The $J[R]$ integral is then recalled and briefly explained in Section 6. It is being used in conjunction with the numerically computed dual functions and their shadows to extract ESIFs from p-FE solutions. Two examples are provided – a crack in an isotropic domain for which the analytical solution is known, and a crack in an anisotropic domain. The extracted ESIFs are shown to be accurate and methods are efficient.
- We conclude by a summary in Section 7.

2. Elastic solution in the vicinity of an edge

2.1. Notations and the differential equations

Consider a domain Ω in which one straight edge $\mathscr{E}$ of interest is present. For simplicity of presentation let the domain be generated as the product $\Omega = G \times I$ where I is the interval $[-1,1]$, and G is a plane bounded sector of opening $\omega \in (0, 2\pi]$ with a radius 1 (the case of a crack, $\omega = 2\pi$, is included), as shown in Fig. 1. Of course any G or I can be chosen and these simplified ones have been chosen for simplicity of presentation.

The variables in G and I are (x_1, x_2) and x_3 respectively, and the coordinates (x_1, x_2, x_3) are denoted by $\boldsymbol{x}$. Let (r, θ) be the polar coordinates centered at the vertex of G so that G coincides with $\{(x_1, x_2) \in \mathbb{R}^2 | r \in (0,1), \theta \in (0, \omega)\}$. The *edge* $\mathscr{E}$ of interest is the set $\{\boldsymbol{x} \in \mathbb{R}^3 \mid r = 0, x_3 \in I\}$. The two flat planes that intersect at the edge $\mathscr{E}$ are denoted by Γ_1 and Γ_2. For any R, $0 < R < 1$, the cylindrical surface Γ_R is defined as follows:

$$\Gamma_R := \{\boldsymbol{x} \in \mathbb{R}^3 | r = R, \theta \in (0, \omega), x_3 \in I\}. \tag{1}$$

Remark 1. The methods presented in the paper are restricted to geometries where the edges are straight lines and the angle ω is fixed along x_3. For a non-fixed ω along x_3, the eigen-values are also x_3 dependent and therefore the theorem presented herein (see Theorem 1 in the sequel) is not applicable.

Remark 2. In general the eigen-pairs associated with the elasticity operator may be complex which add another level of technical complexity. Herein, for simplicity of presentation, we concentrate our attention on cases for which the eigen-values smaller than 1 are real. Nevertheless, the application of the method for complex eigen-values is conceptually the same and will be addressed in a future publication.

To distinguish between the displacement vector in Cartesian or Polar coordinates, we denote these by $\boldsymbol{u} = \{u_1, u_2, u_3\}^{\mathrm{T}}, \tilde{\boldsymbol{u}} = \{u_r, u_\theta, u_{x_3}\}^{\mathrm{T}}$, respectively and use either of them when convenient. The strains and stresses are denoted by $\boldsymbol{\varepsilon} = \{\varepsilon_{11}, \varepsilon_{22}, \varepsilon_{33}, \gamma_{23}, \gamma_{13}, \gamma_{12}\}^{\mathrm{T}}, \tilde{\boldsymbol{\varepsilon}} = \{\varepsilon_{rr}, \varepsilon_{\theta\theta}, \varepsilon_{33}, \gamma_{\theta 3}, \gamma_{r3}, \gamma_{r\theta}\}^{\mathrm{T}}$ and $\boldsymbol{\sigma} = \{\sigma_{11}, \sigma_{22}, \sigma_{33}, \sigma_{23}, \sigma_{13}, \sigma_{12}\}^{\mathrm{T}}$, $\tilde{\boldsymbol{\sigma}} = \{\sigma_{rr}, \sigma_{\theta\theta}, \sigma_{33}, \sigma_{\theta 3}, \sigma_{r3}, \sigma_{r\theta}\}^{\mathrm{T}}$.

For a general anisotropic domain Hooke's law is given by

$$\tilde{\boldsymbol{\sigma}} = \mathbf{C}\tilde{\boldsymbol{\varepsilon}}, \quad \mathbf{C} = \begin{pmatrix} C_{11} & C_{12} & C_{13} & C_{14} & C_{15} & C_{16} \\ & C_{22} & C_{23} & C_{24} & C_{25} & C_{26} \\ & & C_{33} & C_{34} & C_{35} & C_{36} \\ & & & C_{44} & C_{45} & C_{46} \\ & & & & C_{55} & C_{56} \\ & & & & & C_{66} \end{pmatrix}, \tag{2}$$

where C_{ij} are the material properties of the anisotropic domain. The Navier–Lamé (N–L) equations for an elastic anisotropic domain without body forces in cylindrical coordinates are

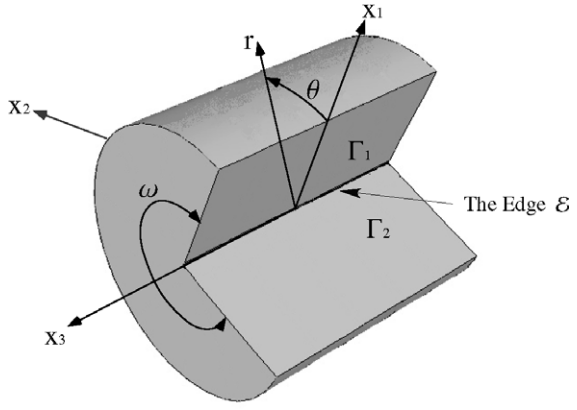

Fig. 1. Domain of interest Ω.

$$\left(-C_{22}\frac{1}{r}+C_{15}\partial_3+C_{55}r\partial_3^2+2C_{56}\partial_\theta\partial_3+C_{66}\frac{1}{r}\partial_\theta^2+C_{11}\partial_r+2C_{15}r\partial_r\partial_3+2C_{16}\partial_r\partial_\theta+C_{11}r\partial_r^2\right)u_r$$
$$+\left(C_{26}\frac{1}{r}+(C_{14}-C_{24}-C_{56})\partial_3+C_{45}r\partial_3^2-(C_{22}+C_{66})\frac{1}{r}\partial_\theta+(C_{25}+C_{46})\partial_\theta\partial_3+C_{26}\frac{1}{r}\partial_\theta^2-C_{26}\partial_r\right.$$
$$\left.+(C_{14}+C_{56})r\partial_r\partial_3+(C_{12}+C_{66})\partial_r\partial_\theta+C_{16}r\partial_r^2\right)u_\theta+\left((C_{13}-C_{23})\partial_3+C_{35}r\partial_3^2-C_{24}\frac{1}{r}\partial_\theta\right.$$
$$\left.+(C_{36}+C_{45})\partial_\theta\partial_3+C_{46}\frac{1}{r}\partial_\theta^2+(C_{15}-C_{25})\partial_r+(C_{13}+C_{55})r\partial_r\partial_3+(C_{14}+C_{56})\partial_r\partial_\theta+C_{15}r\partial_r^2\right)u_3=0. \tag{3}$$

$$\left(C_{26}\frac{1}{r}+(C_{24}+2C_{56})\partial_3+C_{45}r\partial_3^2+(C_{22}+C_{66})\frac{1}{r}\partial_\theta+(C_{25}+C_{46})\partial_\theta\partial_3+C_{26}\frac{1}{r}\partial_\theta^2+(2C_{16}+C_{26})\partial_r\right.$$
$$\left.+(C_{14}+C_{56})r\partial_r\partial_3+(C_{12}+C_{66})\partial_r\partial_\theta+C_{16}r\partial_r^2\right)u_r+\left(-C_{66}\frac{1}{r}+C_{46}\partial_3+C_{44}r\partial_3^2+2C_{24}\partial_\theta\partial_3\right.$$
$$\left.+C_{22}\frac{1}{r}\partial_\theta^2+C_{66}\partial_r+2C_{46}r\partial_r\partial_3+2C_{26}\partial_r\partial_\theta+C_{66}r\partial_r^2\right)u_\theta+\left(2C_{36}\partial_3+C_{34}r\partial_3^2+C_{46}\frac{1}{r}\partial_\theta\right.$$
$$\left.+(C_{23}+C_{44})\partial_\theta\partial_3+C_{24}\frac{1}{r}\partial_\theta^2+2C_{56}\partial_r+(C_{36}+C_{45})r\partial_r\partial_3+(C_{25}+C_{46})\partial_r\partial_\theta+C_{56}r\partial_r^2\right)u_3=0. \tag{4}$$

$$\left((C_{23}+C_{55})\partial_3+C_{35}r\partial_3^2+C_{24}\frac{1}{r}\partial_\theta+(C_{36}+C_{45})\partial_\theta\partial_3+C_{46}\frac{1}{r}\partial_\theta^2+(C_{15}+C_{25})\partial_r+(C_{13}+C_{55})r\partial_r\partial_3\right.$$
$$\left.+(C_{14}+C_{56})\partial_r\partial_\theta+C_{15}r\partial_r^2\right)u_r+\left((C_{45}-C_{36})\partial_3+C_{34}r\partial_3^2-C_{46}\frac{1}{r}\partial_\theta+(C_{23}+C_{44})\partial_\theta\partial_3\right.$$
$$\left.+C_{24}\frac{1}{r}\partial_\theta^2+(C_{36}+C_{45})r\partial_r\partial_3+(C_{25}+C_{46})\partial_r\partial_\theta+C_{56}r\partial_r^2\right)u_\theta+\left(C_{35}\partial_3+C_{33}r\partial_3^2\right.$$
$$\left.+2C_{34}\partial_\theta\partial_3+C_{44}\frac{1}{r}\partial_\theta^2+C_{55}\partial_r+2C_{35}r\partial_r\partial_3+2C_{45}\partial_r\partial_\theta+C_{55}r\partial_r^2\right)u_3=0. \tag{5}$$

The system (3)–(5) can be split into three operators, each being a function of r,θ alone (see [14,8,4]):

$$\mathscr{L}(\tilde{\boldsymbol{u}})=[M_0(\partial_r,\partial_\theta)]\tilde{\boldsymbol{u}}+[M_1(\partial_r,\partial_\theta)]\partial_3\tilde{\boldsymbol{u}}+[M_2(\partial_r,\partial_\theta)]\partial_3^2\tilde{\boldsymbol{u}}=0. \tag{6}$$

2.2. The series expansion of the primal and dual solutions

The splitting (6) allows an expression of the solution $\tilde{\boldsymbol{u}}$ as a series:

$$\tilde{\boldsymbol{u}}=\sum_{i\geqslant 1}\sum_{j\geqslant 0}\partial_3^j A_i(x_3)\boldsymbol{\Phi}_j^{(\alpha_i)}(r,\theta),\quad \boldsymbol{\Phi}_j^{(\alpha_i)}(r,\theta)=r^{\alpha_i+j}\boldsymbol{\varphi}_j^{(\alpha_i)}(\theta), \tag{7}$$

where $A_i(x_3)$ is the edge stress intensity function (ESIF) associated with the ith eigen-pair, the *primal singular function* $\boldsymbol{\Phi}_0^{(\alpha_i)}=r^{\alpha_i}\boldsymbol{\varphi}_0^{(\alpha_i)}(\theta)$ being the well known two-dimensional eigen-function, whereas $\boldsymbol{\Phi}_j^{(\alpha_i)}$, $j\geqslant 1$ are the *shadow functions* of the primal singular function and are determined by the following recursive relations (see [7,22]):

$$\begin{cases}[M_0]\boldsymbol{\Phi}_0^{(\alpha_i)}=0\\ [M_0]\boldsymbol{\Phi}_1^{(\alpha_i)}+[M_1]\boldsymbol{\Phi}_0^{(\alpha_i)}=0 & (r,\theta)\in G\\ [M_0]\boldsymbol{\Phi}_{j+2}^{(\alpha_i)}+[M_1]\boldsymbol{\Phi}_{j+1}^{(\alpha_i)}+[M_2]\boldsymbol{\Phi}_j^{(\alpha_i)}=0,\quad j\geqslant 0\end{cases} \tag{8}$$

accompanied by homogeneous boundary conditions on the two surfaces Γ_1 and Γ_2.

For an isotropic domain, the material matrix $\mathbf{C}$ is determined by two material properties E,ν, and system (3)–(5) is considerably simplified. For this case the eigen-values α_i, eigen-functions $\boldsymbol{\Phi}_0$ and their shadows $\boldsymbol{\Phi}_1,\boldsymbol{\Phi}_2,\ldots$ can be computed analytically as provided in [22]. However, in general these have to be computed by numerical methods discussed herein.

Because the N–L operator is self-adjoint, for any real eigen-value α_i also $-\alpha_i$ is an eigen-value with an associated eigen-function $\boldsymbol{\Phi}_0^{(-\alpha_i)}$ and its shadows $\boldsymbol{\Phi}_j^{(-\alpha_i)}$. Solutions of (8) for the *negative eigen-values* $-\alpha_i$ are called the *dual singular solutions*, and are denoted by $\boldsymbol{\Psi}_j^{(\alpha_i)}$. For normalization purpose a real coefficient $c_0^{(\alpha_i)}$ is chosen, linking $\boldsymbol{\Phi}_j^{(\alpha_i)}$ with $\boldsymbol{\Psi}_j^{(\alpha_i)}$:

$$\boldsymbol{\Psi}_0^{(\alpha_i)}=r^{-\alpha_i}\boldsymbol{\psi}_0^{(\alpha_i)}(\theta)=c_0^{(\alpha_i)}r^{-\alpha_i}\boldsymbol{\varphi}_0^{(-\alpha_i)}(\theta) \tag{9}$$

and

$$\mathbf{\Psi}_j^{(\alpha_i)} = r^{-\alpha_i+j}\boldsymbol{\psi}_j^{(\alpha_i)}(\theta) = r^{-\alpha_i+j}\boldsymbol{\varphi}_j^{(-\alpha_i)}(\theta). \tag{10}$$

Theoretical details and rigorous mathematical formulation are provided in [7]. Detailed explanation about the shadow functions for isotropic domains is presented in [22].

2.3. Boundary conditions for the primal and dual shadow functions

Either traction free or clamped boundary conditions are considered on Γ_1 and Γ_2.

2.3.1. Traction free boundary conditions

Traction free boundary conditions on Γ_1, Γ_2 are

$$[T](\tilde{\boldsymbol{u}})|_{\Gamma_1,\Gamma_2} = ([T_0(\partial_r,\partial_\theta)]\tilde{\boldsymbol{u}} + [T_1(\partial_r,\partial_\theta)]\partial_3\tilde{\boldsymbol{u}})|_{\Gamma_1,\Gamma_2} = 0. \tag{11}$$

Inserting (7) in (11) one obtains the following conditions for the eigen-functions:

$$\begin{cases} [T_0]\mathbf{\Phi}_0 = 0 \\ [T_0]\mathbf{\Phi}_{j+1} + [T_1]\mathbf{\Phi}_j = 0, \quad j \geqslant 0 \end{cases} \quad \text{on } \Gamma_1, \Gamma_2. \tag{12}$$

Explicit expressions for $[T_0]$ and $[T_1]$ for an anisotropic material are

$$\begin{aligned}
\{\sigma_{r\theta}\}|_{\theta=0,\omega} &= \{(C_{26} + C_{56}r\partial_3 + C_{66}\partial_\theta + C_{16}r\partial_r)u_r + (-C_{66} + C_{46}r\partial_3 + C_{26}\partial_\theta + C_{66}r\partial_r)u_\theta \\
&\quad + (C_{36}r\partial_3 + C_{46}\partial_\theta + C_{56}r\partial_r)u_3\}|_{\theta=0,\omega} = 0, \\
\{\sigma_{\theta\theta}\}|_{\theta=0,\omega} &= \{(C_{22} + C_{25}r\partial_3 + C_{26}\partial_\theta + C_{12}r\partial_r)u_r + (-C_{26} + C_{24}r\partial_3 + C_{22}\partial_\theta + C_{26}r\partial_r)u_\theta \\
&\quad + (C_{23}r\partial_3 + C_{24}\partial_\theta + C_{25}r\partial_r)u_3\}|_{\theta=0,\omega} = 0, \\
\{\sigma_{\theta 3}\}|_{\theta=0,\omega} &= \{(C_{24} + C_{45}r\partial_3 + C_{46}\partial_\theta + C_{14}r\partial_r)u_r + (-C_{46} + C_{44}r\partial_3 + C_{24}\partial_\theta + C_{46}r\partial_r)u_\theta \\
&\quad + (C_{34}r\partial_3 + C_{44}\partial_\theta + C_{45}r\partial_r)u_3\}|_{\theta=0,\omega} = 0.
\end{aligned} \tag{13}$$

2.3.2. Clamped boundary conditions

Clamped boundary conditions on Γ_1, Γ_2 are

$$\mathbf{\Phi}_j(r,\theta) = 0 \quad \text{on } \Gamma_1, \Gamma_2. \tag{14}$$

For anisotropic materials, analytical expressions for the eigen-pairs (which are smooth functions in θ) are unavailable due to the untractable mathematical problem, therefore numerical methods are sought. The p-version of the finite element method (FEM) is applied because of the proven exponential convergence rates for smooth solutions [19].

3. Computation of eigen-pairs

3.1. Weak formulation for computing the primal eigen-pair $\boldsymbol{\alpha}$ and $\mathbf{\Phi}_0$

Any eigen-value α and primal eigen-functions $r^\alpha\boldsymbol{\varphi}_0^{(\alpha)}$ (and dual eigen-functions $r^{-\alpha}\boldsymbol{\psi}_0^{(\alpha)}$) are the solution of the first equation in (8). One may notice that after substituting $r^\alpha\boldsymbol{\varphi}_0^{(\alpha)}$ for $\mathbf{\Phi}_0$ the dependency on r disappears, and an ODE in θ has to be solved:

$$[A_1^0]\boldsymbol{\varphi}_0'' + (\alpha[A_2^0] + [A_3^0])\boldsymbol{\varphi}_0' + (\alpha^2[A_4^0] + \alpha[A_5^0] + [A_6^0])\boldsymbol{\varphi}_0 = 0, \quad \theta \in (0,\omega), \tag{15}$$

which is a quadratic eigen-value problem. The matrices $[A_i^0]$ are generated by the material properties:

$$[A_1^0]=\begin{pmatrix} C_{66} & C_{26} & C_{46} \\ C_{26} & C_{22} & C_{24} \\ C_{46} & C_{24} & C_{44} \end{pmatrix},\quad [A_2^0]=\begin{pmatrix} 2C_{16} & C_{12}+C_{66} & C_{14}+C_{56} \\ C_{12}+C_{66} & 2C_{26} & C_{25}+C_{46} \\ C_{14}+C_{56} & C_{25}+C_{46} & 2C_{45} \end{pmatrix},$$

$$[A_3^0]=\begin{pmatrix} 0 & -C_{22}-C_{66} & -C_{24} \\ C_{22}+C_{66} & 0 & C_{46} \\ C_{24} & -C_{46} & 0 \end{pmatrix},\quad [A_4^0]=\begin{pmatrix} C_{11} & C_{16} & C_{15} \\ C_{16} & C_{66} & C_{56} \\ C_{15} & C_{56} & C_{55} \end{pmatrix},$$

$$[A_5^0]=\begin{pmatrix} 0 & -C_{16}-C_{26} & -C_{25} \\ C_{16}+C_{26} & 0 & C_{56} \\ C_{25} & -C_{56} & 0 \end{pmatrix},\quad [A_6^0]=\begin{pmatrix} -C_{22} & C_{26} & 0 \\ C_{26} & -C_{66} & 0 \\ 0 & 0 & 0 \end{pmatrix}. \tag{16}$$

For traction free boundary conditions, the first equation in (12) is

$$\{[B_1^0]\boldsymbol{\varphi}_0' + (\alpha[B_2^0]+[B_3^0])\boldsymbol{\varphi}_0\}_{\theta=0,\omega}=0, \tag{17}$$

where

$$[B_1^0]=[A_1^0],\quad [B_2^0]=\begin{pmatrix} C_{16} & C_{66} & C_{56} \\ C_{12} & C_{26} & C_{25} \\ C_{14} & C_{46} & C_{45} \end{pmatrix},\quad [B_3^0]=\begin{pmatrix} C_{26} & -C_{66} & 0 \\ C_{22} & -C_{26} & 0 \\ C_{24} & -C_{46} & 0 \end{pmatrix}. \tag{18}$$

For homogeneous Dirichlet boundary conditions one has

$$\{\boldsymbol{\varphi}_0\}|_{\theta=0,\omega}=0. \tag{19}$$

To obtain the weak form we multiply (15) by a test function $\boldsymbol{v}$, integrate over a circular path Γ_R, and using an integration by parts for the second derivative term one obtains:

$$\left\{\{[A_1^0]\boldsymbol{\varphi}_0'\}^{\mathrm{T}}\boldsymbol{v}\right\}_{\theta=0,\omega}-\int_0^{\omega}\{[A_1^0]\boldsymbol{\varphi}_0'\}^{\mathrm{T}}\boldsymbol{v}'\,\mathrm{d}\theta+\int_0^{\omega}\{(\alpha[A_2^0]+[A_3^0])\boldsymbol{\varphi}_0'\}^{\mathrm{T}}\boldsymbol{v}\,\mathrm{d}\theta+\int_0^{\omega}\{(\alpha^2[A_4^0]+\alpha[A_5^0]+[A_6^0])\boldsymbol{\varphi}_0\}^{\mathrm{T}}\boldsymbol{v}\,\mathrm{d}\theta=0.$$

If traction free boundary conditions are prescribed then

$$\left\{\{[A_1^0]\boldsymbol{\varphi}_0'\}^{\mathrm{T}}\boldsymbol{v}\right\}_{\theta=0,\omega}=\left\{\{[B_1^0]\boldsymbol{\varphi}_0'\}^{\mathrm{T}}\boldsymbol{v}\right\}_{\theta=0,\omega}=-\left\{\{(\alpha[B_2^0]+[B_3^0])\boldsymbol{\varphi}_0\}^{\mathrm{T}}\boldsymbol{v}\right\}_{\theta=0,\omega}, \tag{20}$$

otherwise, if homogeneous Dirichlet boundary conditions are applied then

$$\{\boldsymbol{\varphi}_0\}_{\theta=0,\omega}=\{\boldsymbol{v}\}_{\theta=0,\omega}=0\Rightarrow\left\{\{[A_1^0]\boldsymbol{\varphi}_0'\}^{\mathrm{T}}\boldsymbol{v}\right\}_{\theta=0,\omega}=0 \tag{21}$$

and we restrict the space in which the solution is sought. Therefore the weak eigen-formulation for the primal and dual eigen-pairs is

$$\begin{aligned}&\text{Seek } \alpha\in\mathbb{C}, 0\neq\boldsymbol{\varphi}_0\in H^1(0,\omega),\ \text{s.t. } \forall\boldsymbol{v}\in H^1(0,\omega)\\ &(\mathscr{B}_0^0(\boldsymbol{\varphi}_0,\boldsymbol{v})+\mathscr{B}_0^{0(BC)}(\boldsymbol{\varphi}_0,\boldsymbol{v}))+\alpha(\mathscr{B}_1^0(\boldsymbol{\varphi}_0,\boldsymbol{v})+\mathscr{B}_1^{0(BC)}(\boldsymbol{\varphi}_0,\boldsymbol{v}))+\alpha^2\mathscr{B}_2^0(\boldsymbol{\varphi}_0,\boldsymbol{v})=0,\end{aligned} \tag{22}$$

where H^1 is the Sobolev space and

$$\begin{aligned}
\mathscr{B}_0^0(\boldsymbol{\varphi}_0,\boldsymbol{v}) &= -\int_0^\omega \{[A_1^0]\boldsymbol{\varphi}_0'\}^{\mathrm{T}}\boldsymbol{v}'\,\mathrm{d}\theta + \int_0^\omega \{[A_3^0]\boldsymbol{\varphi}_0'\}^{\mathrm{T}}\boldsymbol{v}\,\mathrm{d}\theta + \int_0^\omega \{[A_6^0]\boldsymbol{\varphi}_0\}^{\mathrm{T}}\boldsymbol{v}\,\mathrm{d}\theta,\\
\mathscr{B}_1^0(\boldsymbol{\varphi}_0,\boldsymbol{v}) &= \int_0^\omega \{[A_2^0]\boldsymbol{\varphi}_0'\}^{\mathrm{T}}\boldsymbol{v}\,\mathrm{d}\theta + \int_0^\omega \{[A_5^0]\boldsymbol{\varphi}_0\}^{\mathrm{T}}\boldsymbol{v}\,\mathrm{d}\theta,\\
\mathscr{B}_2^0(\boldsymbol{\varphi}_0,\boldsymbol{v}) &= \int_0^\omega \{[A_4^0]\boldsymbol{\varphi}_0\}^{\mathrm{T}}\boldsymbol{v}\,\mathrm{d}\theta,\\
\mathscr{B}_0^{0(BC)}(\boldsymbol{\varphi}_0,\boldsymbol{v}) &= \begin{cases} -\left\{\{[B_3^0]\boldsymbol{\varphi}_0\}^{\mathrm{T}}\boldsymbol{v}\right\}|_{\theta=0,\omega} & \text{Traction free B.C.},\\ 0 \quad \text{Clamped B.C.}, \end{cases}\\
\mathscr{B}_1^{0(BC)}(\boldsymbol{\varphi}_0,\boldsymbol{v}) &= \begin{cases} -\left\{\{[B_2^0]\boldsymbol{\varphi}_0\}^{\mathrm{T}}\boldsymbol{v}\right\}|_{\theta=0,\omega} & \text{Traction free B.C.},\\ 0 \quad \text{Clamped B.C.} \end{cases}
\end{aligned} \tag{23}$$

For clamped boundary conditions the Sobolev space H^1 is replaced by $\overset{\circ}{H}{}^1 = \{\boldsymbol{v}|\boldsymbol{v}\in H^1, \boldsymbol{v}(\theta=0,\omega)=\vec{0}\}$.

3.2. p-FEMs for the solution of the weak eigen-formulation

We apply p-FEMs for the solution of (22). To this end $\boldsymbol{\varphi}_0 = (\,u_0 \quad v_0 \quad w_0\,)^{\mathrm{T}}$ is expressed in terms of the basis functions $N_k(\xi)$ (integrals of Legendre polynomials) in the standard element:

$$u_0(\xi) = \sum_{k=1}^{p+1} a_k N_k(\xi), \quad v_0(\xi) = \sum_{k=1}^{p+1} a_{p+1+k} N_k(\xi), \quad w_0(\xi) = \sum_{k=1}^{p+1} a_{2p+2+k} N_k(\xi) \tag{24}$$

or

$$\boldsymbol{\varphi}_0 = \begin{pmatrix} N_1(\xi)\cdots N_{p+1}(\xi) & 0\cdots 0 & 0\cdots 0\\ 0\cdots 0 & N_1(\xi)\cdots N_{p+1}(\xi) & 0\cdots 0\\ 0\cdots 0 & 0\cdots 0 & N_1(\xi)\cdots N_{p+1}(\xi) \end{pmatrix} \begin{pmatrix} a_1\\ \vdots\\ a_{3(p+1)} \end{pmatrix} \underset{=}{\mathrm{def}} [N]\boldsymbol{a}_0. \tag{25}$$

Similarly $\boldsymbol{v} \overset{\mathrm{def}}{=} [N]\mathbf{b}_0$, and $\mathrm{d}\theta = \frac{\omega}{2}\,\mathrm{d}\xi$. Substituting (25) in (22) one obtains the FE formulation of the weak eigen-form:

$$\boldsymbol{a}_0^{\mathrm{T}}\left(\alpha^2[K_2^0] + \alpha[K_1^0] + [K_0^0]\right) = \vec{0}, \tag{26}$$

where

$$\begin{aligned}
[K_2^0] &= \frac{\omega}{2}\int_{-1}^{1} [N]^{\mathrm{T}}[A_4^0]^{\mathrm{T}}[N]\,\mathrm{d}\xi,\\
[K_1^0] &= -\left\{[N]^{\mathrm{T}}[B_2^0]^{\mathrm{T}}[N]\right\}_{\theta=0,\omega} + \int_{-1}^{1} [N']^{\mathrm{T}}[A_2^0]^{\mathrm{T}}[N]\,\mathrm{d}\xi + \frac{\omega}{2}\int_{-1}^{1} [N]^{\mathrm{T}}[A_5^0]^{\mathrm{T}}[N]\,\mathrm{d}\xi,\\
[K_0^0] &= -\left\{[N]^{\mathrm{T}}[B_3^0]^{\mathrm{T}}[N]\right\}_{\theta=0,\omega} - \frac{2}{\omega}\int_{-1}^{1} [N']^{\mathrm{T}}[A_1^0]^{\mathrm{T}}[N']\,\mathrm{d}\xi + \int_{-1}^{1} [N']^{\mathrm{T}}[A_3^0]^{\mathrm{T}}[N]\,\mathrm{d}\xi\\
&\quad + \frac{\omega}{2}\int_{-1}^{1} [N]^{\mathrm{T}}[A_6^0]^{\mathrm{T}}[N]\,\mathrm{d}\xi.
\end{aligned} \tag{27}$$

For clamped boundary conditions $[B_2^0] = [B_3^0] = [0]$. The quadratic matrix eigen-problem (26) is solved by a proper linearization process, see [1]. Setting $\boldsymbol{d}_0 = \alpha\boldsymbol{a}_0$ the $(3p+3)\times(3p+3)$ quadratic eigen-problem is transformed into a linear $(6p+6)\times(6p+6)$ "standard matrix eigen-problem":

$$\begin{pmatrix} \boldsymbol{a}_0\\ \boldsymbol{d}_0 \end{pmatrix}^{\mathrm{T}} \begin{pmatrix} 0 & [K_0^0]\\ I & [K_1^0] \end{pmatrix} = \alpha \begin{pmatrix} \boldsymbol{a}_0\\ \boldsymbol{d}_0 \end{pmatrix}^{\mathrm{T}} \begin{pmatrix} I & 0\\ 0 & -[K_2^0] \end{pmatrix}. \tag{28}$$

3.3. The normalization factor c_0

The dual eigen-functions $\boldsymbol{\psi}_0$ are obtained by solving (28) – these are associated with the negative eigen-values. The normalization factor $c_0^{(\alpha)}$ is determined so that the primal and dual eigen-functions satisfy an orthonormal condition (see [7,22]) under the integration along a circular curve with the edge being its center:

$$\int_0^{\omega} \{\boldsymbol{T}^{\Gamma_R}\boldsymbol{\Phi}_0^{(\alpha)} \cdot \boldsymbol{\Psi}_0^{(\alpha)} - \boldsymbol{\Phi}_0^{(\alpha)} \cdot \boldsymbol{T}^{\Gamma_R}\boldsymbol{\Psi}_0^{(\alpha)}\} R \,\mathrm{d}\theta = 1, \tag{29}$$

where $\boldsymbol{T}^{\Gamma_R}$ is Neumann trace operator (related with $\mathscr{L}$) on a circular surface around the edge:

$$\boldsymbol{T}^{\Gamma_R}\tilde{\boldsymbol{u}} \stackrel{\text{def}}{=} \begin{pmatrix} \sigma_{rr} \\ \sigma_{r\theta} \\ \sigma_{r3} \end{pmatrix} = \begin{pmatrix} \frac{1}{r}C_{12} + C_{15}\partial_3 + \frac{1}{r}C_{16}\partial_\theta + C_{11}\partial_r & -\frac{1}{r}C_{16} + C_{14}\partial_3 + \frac{1}{r}C_{12}\partial_\theta + C_{16}\partial_r & C_{13}\partial_3 + \frac{1}{r}C_{14}\partial_\theta + C_{15}\partial_r \\ \frac{1}{r}C_{26} + C_{56}\partial_3 + \frac{1}{r}C_{66}\partial_\theta + C_{16}\partial_r & -\frac{1}{r}C_{66} + C_{46}\partial_3 + \frac{1}{r}C_{26}\partial_\theta + C_{66}\partial_r & C_{36}\partial_3 + \frac{1}{r}C_{46}\partial_\theta + C_{56}\partial_r \\ \frac{1}{r}C_{25} + C_{55}\partial_3 + \frac{1}{r}C_{56}\partial_\theta + C_{15}\partial_r & -\frac{1}{r}C_{56} + C_{45}\partial_3 + \frac{1}{r}C_{25}\partial_\theta + C_{56}\partial_r & C_{35}\partial_3 + \frac{1}{r}C_{45}\partial_\theta + C_{55}\partial_r \end{pmatrix} \begin{pmatrix} u_r \\ u_\theta \\ u_3 \end{pmatrix}. \tag{30}$$

We split the operator $\boldsymbol{T}^{\Gamma_R}$:

$$\boldsymbol{T}^{\Gamma_R} = \boldsymbol{T}_0^{\Gamma_R}(\partial_r, \partial_\theta) + \boldsymbol{T}_1^{\Gamma_R}(\partial_r, \partial_\theta)\partial_3 \tag{31}$$

such that

$$\begin{aligned} \boldsymbol{T}_0^{\Gamma_R}(\partial_r, \partial_\theta)\boldsymbol{\Phi}_j &= \left([T_a]\frac{1}{r}\partial_\theta + [T_b]\partial_r + ([T_c] + j[T_b])\frac{1}{r}\right)\boldsymbol{\Phi}_j, \\ \boldsymbol{T}_1^{\Gamma_R}(\partial_r, \partial_\theta)\boldsymbol{\Phi}_j &= [T_d]\boldsymbol{\Phi}_j, \end{aligned} \tag{32}$$

$$[T_a] = \begin{pmatrix} C_{16} & C_{12} & C_{14} \\ C_{66} & C_{26} & C_{46} \\ C_{56} & C_{25} & C_{45} \end{pmatrix}, \quad [T_b] = \begin{pmatrix} C_{11} & C_{16} & C_{15} \\ C_{16} & C_{66} & C_{56} \\ C_{15} & C_{56} & C_{55} \end{pmatrix}, \quad [T_c] = \begin{pmatrix} C_{12} & -C_{16} & 0 \\ C_{26} & -C_{66} & 0 \\ C_{25} & -C_{56} & 0 \end{pmatrix}, \quad [T_d] = \begin{pmatrix} C_{15} & C_{14} & C_{13} \\ C_{56} & C_{46} & C_{36} \\ C_{55} & C_{45} & C_{35} \end{pmatrix}. \tag{33}$$

Because the eigen-pairs and their duals are independent of x_3 one obtains:

$$\begin{aligned} \boldsymbol{T}^{\Gamma_R}\boldsymbol{\Phi}_0^{(\alpha)} &= \boldsymbol{T}_0^{\Gamma_R}\boldsymbol{\Phi}_0^{(\alpha)} = R^{\alpha-1}\{[T_a]\boldsymbol{\varphi}_0' + \alpha[T_b]\boldsymbol{\varphi}_0 + [T_c]\boldsymbol{\varphi}_0\}, \\ \boldsymbol{T}^{\Gamma_R}\boldsymbol{\Psi}_0^{(\alpha)} &= \boldsymbol{T}_0^{\Gamma_R}\boldsymbol{\Psi}_0^{(\alpha)} = R^{-\alpha-1}\{[T_a]\boldsymbol{\psi}_0' - \alpha[T_b]\boldsymbol{\psi}_0 + [T_c]\boldsymbol{\psi}_0\}. \end{aligned} \tag{34}$$

Inserting (9) into (29), and using (34) one obtain the expression for the normalization factor c_0:

$$c_0^{(\alpha)} = \left[\int_0^{\omega} \{([T_a]\boldsymbol{\varphi}_0' + \alpha[T_b]\boldsymbol{\varphi}_0 + [T_c]\boldsymbol{\varphi}_0) \cdot \boldsymbol{\psi}_0 - \boldsymbol{\varphi}_0 \cdot ([T_a]\boldsymbol{\psi}_0' - \alpha[T_b]\boldsymbol{\psi}_0 + [T_c]\boldsymbol{\psi}_0)\} \,\mathrm{d}\theta\right]^{-1}. \tag{35}$$

4. Computation of the primal and dual shadow functions

4.1. Weak formulation for computing the primal and dual first shadow functions, $\boldsymbol{\Phi}_1$ and $\boldsymbol{\Psi}_1$

The primal shadow functions $\boldsymbol{\varphi}_1$, presented in (7), as well as the dual shadow function $\boldsymbol{\psi}_1$ are the solution of the second differential equation in (8).

Remark 3. The method presented herein addresses $\boldsymbol{\varphi}_1$. The method is applicable to $\boldsymbol{\psi}_1$ by replacing $\boldsymbol{\varphi}_1$, $\boldsymbol{\varphi}_0$ and α with $\boldsymbol{\psi}_1$, $\boldsymbol{\psi}_0$ and $-\alpha$. Notice that the eigen-value α is known, obtained by solving the eigen-value problem in the previous chapter. The unknown functions $\boldsymbol{\varphi}_1$ and $\boldsymbol{\psi}_1$ are obtained by solving the second differential equation in (8).

After substituting $r^{\alpha}\boldsymbol{\varphi}_0^{(\alpha)}$ for $\boldsymbol{\Phi}_0$ and $r^{\alpha+1}\boldsymbol{\varphi}_1^{(\alpha)}$ for $\boldsymbol{\Phi}_1$ in the second equation of (8), the dependency on r disappears, and an ODE in θ has to be solved:

$$[A_1^0]\boldsymbol{\varphi}_1'' + (\alpha[A_2^0] + [A_3^1])\boldsymbol{\varphi}_1' + (\alpha^2[A_4^0] + \alpha[A_5^1] + [A_6^1])\boldsymbol{\varphi}_1 + [A_7^1]\boldsymbol{\varphi}_0' + (\alpha[A_8^1] + [A_9^1]\boldsymbol{\varphi}_0) = \vec{0}. \tag{36}$$

The matrices $[A_i^1]$ depend on the material constants:

$$[A_3^1] = \begin{pmatrix} 2C_{16} & (C_{12}-C_{22}) & (C_{14}-C_{24}+C_{56}) \\ (C_{12}+C_{22}+2C_{66}) & 2C_{26} & (C_{25}+2C_{46}) \\ (C_{14}+C_{24}+C_{56}) & C_{25} & 2C_{45} \end{pmatrix},$$

$$[A_5^1] = \begin{pmatrix} 2C_{11} & (C_{16}-C_{26}) & (2C_{15}-C_{25}) \\ (3C_{16}+C_{26}) & 2C_{66} & 3C_{56} \\ (2C_{15}+C_{25}) & C_{56} & 2C_{55} \end{pmatrix}, \quad [A_6^1] = \begin{pmatrix} (C_{11}-C_{22}) & 0 & (C_{15}-C_{25}) \\ 32(C_{16}+C_{26}) & 0 & 2C_{56} \\ (C_{15}+C_{25}) & 0 & C_{55} \end{pmatrix},$$

$$[A_7^1] = \begin{pmatrix} 2C_{56} & (C_{25}+C_{46}) & (C_{36}+C_{45}) \\ (C_{25}+C_{46}) & 2C_{24} & (C_{23}+C_{44}) \\ (C_{36}+C_{45}) & (C_{23}+C_{44}) & 2C_{34} \end{pmatrix}, \quad [A_8^1] = \begin{pmatrix} 2C_{15} & (C_{14}+C_{56}) & (C_{13}+C_{55}) \\ (C_{14}+C_{56}) & 2C_{46} & (C_{36}+C_{45}) \\ (C_{13}+C_{55}) & (C_{36}+C_{45}) & 2C_{35} \end{pmatrix},$$

$$[A_9^1] = \begin{pmatrix} C_{15} & (C_{14}-C_{24}-C_{56}) & (C_{13}-C_{23}) \\ (C_{24}+2C_{56}) & C_{46} & 2C_{36} \\ (C_{23}+C_{55}) & -(C_{36}-C_{45}) & C_{35} \end{pmatrix}. \tag{37}$$

The boundary conditions applied on the two surfaces Γ_1 and Γ_2 may be either traction free on homogeneous Dirichlet. In the case of traction free boundary conditions, the second equation in (12) results in

$$\{[B_1^0]\boldsymbol{\varphi}_1' + (\alpha[B_2^0] + [B_3^1])\boldsymbol{\varphi}_1 + [B_4^1]\boldsymbol{\varphi}_0'\}|_{\theta=0,\omega} = \vec{0} \tag{38}$$

with

$$[B_3^1] = \begin{pmatrix} (C_{16}+C_{26}) & 0 & C_{56} \\ (C_{12}+C_{22}) & 0 & C_{25} \\ (C_{14}+C_{24}) & 0 & C_{45} \end{pmatrix}, \quad [B_4^1] = \begin{pmatrix} C_{56} & C_{46} & C_{36} \\ C_{25} & C_{24} & C_{23} \\ C_{45} & C_{44} & C_{34} \end{pmatrix}. \tag{39}$$

If homogeneous Dirichlet boundary conditions are applied on the two surfaces Γ_1 and Γ_2, then the condition on $\boldsymbol{\varphi}_1$ is

$$\{\boldsymbol{\varphi}_1\}|_{\theta=0,\omega} = \vec{0}. \tag{40}$$

To obtain the weak form associated with the second differential equation in (8) we multiply (36) by a test function $\boldsymbol{v}$ and integrate over a circular path Γ_R, and using an integration by parts for the second derivative term one obtains:

$$\begin{aligned} &\{([A_1^0]\boldsymbol{\varphi}_1')^{\mathrm{T}}\boldsymbol{v}\}|_{\theta=0,\omega} - \int_0^\omega ([A_1^0]\boldsymbol{\varphi}_1')^{\mathrm{T}}\boldsymbol{v}'\,\mathrm{d}\theta + \int_0^\omega [(\alpha[A_2^0] + [A_3^1])\boldsymbol{\varphi}_1']^{\mathrm{T}}\boldsymbol{v}\,\mathrm{d}\theta + \int_0^\omega [(\alpha^2[A_4^0] + \alpha[A_5^1] + [A_6])\boldsymbol{\varphi}_1]^{\mathrm{T}}\boldsymbol{v}\,\mathrm{d}\theta \\ &\quad + \int_0^\omega ([A_7^1]\boldsymbol{\varphi}_0')^{\mathrm{T}}\boldsymbol{v}\,\mathrm{d}\theta + \int_0^\omega [(\alpha[A_8^1] + [A_9^1])\boldsymbol{\varphi}_0]^{\mathrm{T}}\boldsymbol{v}\,\mathrm{d}\theta = 0. \end{aligned} \tag{41}$$

If traction free boundary conditions are prescribed then the first term in (41) is

$$\{([A_1^0]\boldsymbol{\varphi}_1')^{\mathrm{T}}\boldsymbol{v}\}|_{\theta=0,\omega} = \{([B_1^0]\boldsymbol{\varphi}_1')^{\mathrm{T}}\boldsymbol{v}\}|_{\theta=0,\omega} = -\{[(\alpha[B_2^0] + [B_3^1])\boldsymbol{\varphi}_1]^{\mathrm{T}}\boldsymbol{v}\}|_{\theta=0,\omega} - \{([B_4^1]\boldsymbol{\varphi}_0)^{\mathrm{T}}\boldsymbol{v}\}|_{\theta=0,\omega}, \tag{42}$$

otherwise, if homogeneous Dirichlet boundary conditions are applied then

$$\{\boldsymbol{\varphi}_1\}_{\theta=0,\omega} = \{\boldsymbol{v}\}_{\theta=0,\omega} = 0 \Rightarrow \{([A_1^0]\boldsymbol{\varphi}_1')^{\mathrm{T}}\boldsymbol{v}\}_{\theta=0,\omega} = 0 \tag{43}$$

and we restrict the space in which the solution is sought. Therefore the weak formulation for the computation of $\boldsymbol{\varphi}_1$ is

$$\text{Seek } \boldsymbol{\varphi}_1 \in H^1(0,\omega),\ \text{s.t. } \mathscr{B}^1(\boldsymbol{\varphi}_1,\boldsymbol{v}) + \mathscr{B}^{1(BC)}(\boldsymbol{\varphi}_1,\boldsymbol{v}) = \mathscr{F}^1(\boldsymbol{v}) + \mathscr{F}^{1(BC)}(\boldsymbol{v}), \quad \forall \boldsymbol{v} \in H^1(0,\omega), \tag{44}$$

where H^1 is the Sobolev space,

$$\begin{aligned} \mathscr{B}^1(\boldsymbol{\varphi}_1,\boldsymbol{v}) &= -\int_0^\omega ([A_1^0]\boldsymbol{\varphi}_1')^{\mathrm{T}}\boldsymbol{v}'\,\mathrm{d}\theta + \int_0^\omega [(\alpha[A_2^0] + [A_3^1])\boldsymbol{\varphi}_1']^{\mathrm{T}}\boldsymbol{v}\,\mathrm{d}\theta + \int_0^\omega [(\alpha^2[A_4^0] + \alpha[A_5^1] + [A_6^1])\boldsymbol{\varphi}_1]^{\mathrm{T}}\boldsymbol{v}\,\mathrm{d}\theta, \\ \mathscr{B}^{1(BC)}(\boldsymbol{\varphi}_1,\boldsymbol{v}) &= \begin{cases} -\{[(\alpha[B_2^0] + [B_3^1])\boldsymbol{\varphi}_1]^{\mathrm{T}}\boldsymbol{v}\}|_{\theta=0,\omega} & \text{Traction free B.C.,} \\ 0 \quad \text{Clamped B.C.} \end{cases} \end{aligned} \tag{45}$$

and

$$\mathscr{F}^1(\boldsymbol{v}) = -\int_0^\omega ([A_7^1]\boldsymbol{\varphi}_0')^{\mathrm{T}}\boldsymbol{v}\,\mathrm{d}\theta - \int_0^\omega [(\alpha[A_8^1]+[A_9^1])\boldsymbol{\varphi}_0]^{\mathrm{T}}\boldsymbol{v}\,\mathrm{d}\theta,$$
$$\mathscr{F}^{1(BC)}(\boldsymbol{v}) = \begin{cases} \{([B_4^1]\boldsymbol{\varphi}_0)^{\mathrm{T}}\boldsymbol{v}\}|_{\theta=0,\omega} & \text{Traction free B.C.,} \\ 0 \quad \text{Clamped B.C.} \end{cases} \tag{46}$$

For clamped boundary conditions the Sobolev space H^1 is replaced by $\overset{\circ}{H}{}^1 = \{\boldsymbol{v}|\boldsymbol{v}\in H^1, \boldsymbol{v}(\theta=0,\omega)=\vec{0}\}$.

4.2. p-FEMs for the solution of the weak formulation (44)

We apply p-FEMs for the solution of (44) similarly to Section 3.2. To this end $\boldsymbol{\varphi}_1 = (\,u_1 \quad v_1 \quad w_1\,)^{\mathrm{T}} = [N]\boldsymbol{a}_1$ and $\boldsymbol{v} \overset{\text{def}}{=} [N]\boldsymbol{b}_1$. The resulting FE formulation is

$$\boldsymbol{a}_1^{\mathrm{T}}[K^1] = \boldsymbol{F}^1, \tag{47}$$

where

$$[K^1] = -\{[N]^{\mathrm{T}}(\alpha[B_2^0]^{\mathrm{T}}+[B_3^1]^{\mathrm{T}})[N]\}|_{\theta=0,\omega} - \frac{2}{\omega}\int_{-1}^1 [N']^{\mathrm{T}}[A_1^0]^{\mathrm{T}}[N']\,\mathrm{d}\xi + \int_{-1}^1 [N']^{\mathrm{T}}(\alpha[A_2^0]^{\mathrm{T}}+[A_3^1]^{\mathrm{T}})[N]\,\mathrm{d}\xi$$
$$+\frac{\omega}{2}\int_{-1}^1 [N]^{\mathrm{T}}(\alpha^2[A_4^0]^{\mathrm{T}}+\alpha[A_5^1]^{\mathrm{T}}+[A_6^1]^{\mathrm{T}})[N]\,\mathrm{d}\xi,$$
$$\boldsymbol{F}^1 = \{\boldsymbol{a}_0^{\mathrm{T}}[N]^{\mathrm{T}}[B_4^1]^{\mathrm{T}}[N]\}|_{\theta=0,\omega} - \int_{-1}^1 \boldsymbol{a}_0^{\mathrm{T}}[N']^{\mathrm{T}}[A_7^1]^{\mathrm{T}}[N]\,\mathrm{d}\xi - \frac{\omega}{2}\int_{-1}^1 \boldsymbol{a}_0^{\mathrm{T}}[N]^{\mathrm{T}}(\alpha[A_8^1]^{\mathrm{T}}+[A_9^1]^{\mathrm{T}})[N]\,\mathrm{d}\xi. \tag{48}$$

For clamped boundary conditions $[B_2^0]=[B_3^1]=[B_4^1]=[0]$.

4.3. The non-uniqueness of $\boldsymbol{\varphi}_1, \boldsymbol{\psi}_1$ and the $\mathscr{H}_1$ condition

The differential equation for $\boldsymbol{\varphi}_1$ and the differential equation for $\boldsymbol{\psi}_1$ are both non-homogeneous equations, so the solution is a combination of a particular solution and homogeneous solution, i.e.:

$$\boldsymbol{\varphi}_1(\theta) = \boldsymbol{\varphi}_1^{(P)}(\theta) + \boldsymbol{\varphi}_1^{(H)}(\theta), \quad \boldsymbol{\psi}_1(\theta) = \boldsymbol{\psi}_1^{(P)}(\theta) + \boldsymbol{\psi}_1^{(H)}(\theta). \tag{49}$$

The homogeneous solution $\boldsymbol{\varphi}_1^{(H)}(r,\theta)$ and $\boldsymbol{\psi}_1^{(H)}(r,\theta)$ are of the form:

$$\boldsymbol{\varphi}_1^{(H)}(\theta) = C^{\varphi_1}\boldsymbol{\varphi}_0(\theta), \quad \boldsymbol{\psi}_1^{(H)}(\theta) = C^{\psi_1}\boldsymbol{\psi}_0(\theta), \tag{50}$$

where $C^{\varphi_1}, C^{\psi_1} \in \mathbb{R}$. Because C^{φ_1} and C^{ψ_1} are undefined, we may choose any value of C^{φ_1} and C^{ψ_1}, including $C^{\varphi_1}=C^{\psi_1}=0$, and therefore there are an infinite number of $\boldsymbol{\varphi}_1$ and $\boldsymbol{\psi}_1$ functions for which the differential equation hold. However, the shadow function $\boldsymbol{\varphi}_1$ and $\boldsymbol{\psi}_1$ have to satisfy another condition, denoted by $\mathscr{H}_1$ (for further details see [7]):

$$\mathscr{H}_1 = \int_0^\omega \{\boldsymbol{T}_0^{\Gamma_R}\boldsymbol{\Phi}_0\cdot\boldsymbol{\Psi}_1 - \boldsymbol{\Phi}_0\cdot\boldsymbol{T}_0^{\Gamma_R}\boldsymbol{\Psi}_1\}\,\mathrm{d}\theta - \int_0^\omega \{\boldsymbol{T}_0^{\Gamma_R}\boldsymbol{\Phi}_1\cdot\boldsymbol{\Psi}_0 - \boldsymbol{\Phi}_1\cdot\boldsymbol{T}_0^{\Gamma_R}\boldsymbol{\Psi}_0\}\,\mathrm{d}\theta - \int_0^\omega \{\boldsymbol{T}_1^{\Gamma_R}\boldsymbol{\Phi}_0\cdot\boldsymbol{\Psi}_0 - \boldsymbol{\Phi}_0\cdot\boldsymbol{T}_0^{\Gamma_R}\boldsymbol{\Psi}_0\}\,\mathrm{d}\theta = 0, \tag{51}$$

where $\boldsymbol{T}_0^{\Gamma_R}$ and $\boldsymbol{T}_1^{\Gamma_R}$ are given in (32).

Once the functions $\boldsymbol{\varphi}_1$ and $\boldsymbol{\psi}_1$ are computed, $\mathscr{H}_1$ can be evaluated. In case $\mathscr{H}_1 \neq 0$, $\mathscr{H}_1$ is recomputed using

$$\boldsymbol{\psi}_1^{\mathrm{NEW}} = \boldsymbol{\psi}_1 + C^{\psi_1}\boldsymbol{\psi}_0. \tag{52}$$

The constant C^{ψ_1} is chosen such that $\mathscr{H}_1 = 0$.

4.4. Weak formulation for computing the primal and dual second shadow functions, $\boldsymbol{\Phi}_2$ and $\boldsymbol{\Psi}_2$

The primal shadow functions $\boldsymbol{\varphi}_2$ and the dual shadow function $\boldsymbol{\psi}_2$ are the solutions of the third differential equation in (8).

Remark 4. The method presented herein addresses the computation of $\boldsymbol{\varphi}_2$. The method is applicable to $\boldsymbol{\psi}_2$ computation by replacing $\boldsymbol{\varphi}_2, \boldsymbol{\varphi}_1, \boldsymbol{\varphi}_0$ and α with $\boldsymbol{\psi}_2, \boldsymbol{\psi}_1, \boldsymbol{\psi}_0$ and $-\alpha$.

After substituting $r^{\alpha+2}\boldsymbol{\varphi}_2^{(\alpha)}$ for $\boldsymbol{\Phi}_2$, the dependency on r disappears, and an ODE in θ has to be solved:

$$[A_1^0]\boldsymbol{\varphi}_2'' + (\alpha[A_2^0] + [A_3^2])\boldsymbol{\varphi}_2' + (\alpha^2[A_4^0] + \alpha[A_5^2] + [A_6^2])\boldsymbol{\varphi}_2 + [A_7^1]\boldsymbol{\varphi}_1' + (\alpha[A_8^1] + [A_9^2])\boldsymbol{\varphi}_1 + [A_{10}^2]\boldsymbol{\varphi}_0 = 0. \tag{53}$$

The matrices $[A_i^2]$ generated by the material properties are

$$[A_3^2] = \begin{pmatrix} 4C_{16} & (2C_{12} - C_{22} + C_{66}) & (2C_{14} - C_{24} + 2C_{56}) \\ (2C_{12} + C_{22} + 3C_{66}) & 4C_{26} & (2C_{25} + 3C_{46}) \\ (2C_{14} + C_{24} + 2C_{56}) & (2C_{25} + C_{46}) & 4C_{45} \end{pmatrix},$$

$$[A_5^2] = \begin{pmatrix} 4C_{11} & (3C_{16} - C_{26}) & (4C_{15} - C_{25}) \\ (5C_{16} + C_{26}) & 4C_{66} & 5C_{56} \\ (4C_{15} + C_{25}) & 3C_{56} & 4C_{55} \end{pmatrix}, \quad [A_6^2] = \begin{pmatrix} (4C_{11} - C_{22}) & (2C_{16} - C_{26}) & 2(2C_{15} - C_{25}) \\ 3(2C_{16} + C_{26}) & 3C_{66} & 6C_{56} \\ 2(2C_{15} + C_{25}) & 2C_{56} & 4C_{55} \end{pmatrix},$$

$$[A_9^2] = \begin{pmatrix} 3C_{15} & (2C_{14} - C_{24}) & (2C_{13} - C_{23} + C_{55}) \\ (C_{14} + C_{24} + 3C_{56}) & 3C_{46} & (3C_{36} + C_{45}) \\ (C_{13} + C_{23} + 2C_{55}) & 2C_{45} & 3C_{35} \end{pmatrix}, \quad [A_{10}^2] = \begin{pmatrix} C_{55} & C_{45} & C_{35} \\ C_{45} & C_{44} & C_{34} \\ C_{35} & C_{34} & C_{33} \end{pmatrix}. \tag{54}$$

In the case where traction free boundary conditions are applied, the second equation in (12) provides the conditions for $\boldsymbol{\varphi}_2^{(\alpha)}$:

$$\{[B_1^0]\boldsymbol{\varphi}_2' + (\alpha[B_2^0] + [B_3^2])\boldsymbol{\varphi}_2 + [B_4^1]\boldsymbol{\varphi}_1'\}|_{\theta=0,\omega} = \vec{0} \tag{55}$$

with

$$[B_3^2] = \begin{pmatrix} (2C_{16} + C_{26}) & C_{66} & 2C_{56} \\ (2C_{12} + C_{22}) & C_{26} & 2C_{25} \\ (2C_{14} + C_{24}) & C_{46} & 2C_{45} \end{pmatrix}. \tag{56}$$

Thus

$$\begin{aligned} \{([A_1^0]\boldsymbol{\varphi}_2')^{\mathrm{T}}\boldsymbol{v}\}|_{\theta=0,\omega} &= \{([B_1^0]\boldsymbol{\varphi}_2')^{\mathrm{T}}\boldsymbol{v}\}|_{\theta=0,\omega} \\ &= -\{[(\alpha[B_2^0] + [B_3^2])\boldsymbol{\varphi}_2]^{\mathrm{T}}\boldsymbol{v}\}|_{\theta=0,\omega} - \{([B_4^2]\boldsymbol{\varphi}_1)^{\mathrm{T}}\boldsymbol{v}\}|_{\theta=0,\omega}. \end{aligned} \tag{57}$$

If homogeneous Dirichlet boundary conditions are applied on the two surfaces Γ_1 and Γ_2, then the condition on $\boldsymbol{\varphi}_2$ is

$$\{\boldsymbol{\varphi}_2\}|_{\theta=0,\omega} = \vec{0}. \tag{58}$$

Thus

$$\{\boldsymbol{\varphi}_2\}_{\theta=0,\omega} = \{\boldsymbol{v}\}_{\theta=0,\omega} = \vec{0} \Rightarrow \{([A_1^0]\boldsymbol{\varphi}_2')^{\mathrm{T}}\boldsymbol{v}\}_{\theta=0,\omega} = 0. \tag{59}$$

Following the steps in Section 4.1, and using (57) or (59) we obtain the weak form for the function $\boldsymbol{\varphi}_2$:

$$\text{Seek } \boldsymbol{\varphi}_2 \in H^1(0,\omega), \text{ s.t. } \mathscr{B}^2(\boldsymbol{\varphi}_2, \boldsymbol{v}) + \mathscr{B}^{2(BC)}(\boldsymbol{\varphi}_2, \boldsymbol{v}) = \mathscr{F}^2(\boldsymbol{v}) + \mathscr{F}^{2(BC)}(\boldsymbol{v}) \quad \forall \boldsymbol{v} \in H^1(0,\omega), \tag{60}$$

where

$$\mathscr{B}^2(\boldsymbol{\varphi}_2, \boldsymbol{v}) = -\int_0^\omega ([A_1^0]\boldsymbol{\varphi}_2')^{\mathrm{T}}\boldsymbol{v}'\,\mathrm{d}\theta + \int_0^\omega [(\alpha[A_2^0] + [A_3^2]')\boldsymbol{\varphi}_2]^{\mathrm{T}}\boldsymbol{v}\,\mathrm{d}\theta + \int_0^\omega [(\alpha^2[A_4^0] + \alpha[A_5^2] + [A_6^2])\boldsymbol{\varphi}_2]^{\mathrm{T}}\boldsymbol{v}\,\mathrm{d}\theta.$$

$$\mathscr{B}^{2(BC)}(\boldsymbol{\varphi}_2, \boldsymbol{v}) = \begin{cases} -\{[(\alpha[B_2^0] + [B_3^2])\boldsymbol{\varphi}_2]^{\mathrm{T}}\boldsymbol{v}\}|_{\theta=0,\omega} & \text{Traction free B.C.,} \\ 0 \quad \text{Clamped B.C.} \end{cases} \tag{61}$$

and

$$\mathscr{F}^2(\boldsymbol{v}) = -\int_0^\omega ([A_7^1]\boldsymbol{\varphi}_1')^{\mathrm{T}}\boldsymbol{v}\,\mathrm{d}\theta - \int_0^\omega [(\alpha[A_8^1] + [A_9^2])\boldsymbol{\varphi}_1]^{\mathrm{T}}\boldsymbol{v}\,\mathrm{d}\theta - \int_0^\omega ([A_{10}^2]\boldsymbol{\varphi}_0)^{\mathrm{T}}\boldsymbol{v}\,\mathrm{d}\theta.$$

$$\mathscr{F}^{2(BC)}(\boldsymbol{v}) = \begin{cases} \{([B_4^1]\boldsymbol{\varphi}_1)^{\mathrm{T}}\boldsymbol{v}\}|_{\theta=0,\omega} & \text{Traction free B.C.,} \\ 0 \quad \text{Clamped B.C.} \end{cases} \tag{62}$$

For clamped boundary conditions the Sobolev space H^1 is replaced by $\overset{\circ}{H}{}^1 = \{\boldsymbol{v} | \boldsymbol{v} \in H^1, \boldsymbol{v}(\theta = 0, \omega) = \vec{0}\}$.

4.5. p-FEMs for the solution of the weak eigen-formulation

We apply p-FEMs for the solution of (60), similar to Section 3.2, where $\boldsymbol{\varphi}_2 = (\, u_2 \quad v_2 \quad w_2 \,)^{\mathrm{T}} = [N]\boldsymbol{a}_2$ and $\boldsymbol{v} \overset{\text{def}}{=} [N]\boldsymbol{b}_2$. The resulting FE formulation is

$$\boldsymbol{a}_2^{\mathrm{T}}[K^2] = \boldsymbol{F}^2, \tag{63}$$

where

$$\begin{aligned}
[K^2] &= -\{[N]^{\mathrm{T}}(\alpha[B_2^0]^{\mathrm{T}} + [B_3^2])[N]\}|_{\theta=0,\omega} - \frac{2}{\omega}\int_{-1}^{1}[N']^{\mathrm{T}}[A_1^0]^{\mathrm{T}}[N']\,\mathrm{d}\xi + \int_{-1}^{1}[N']^{\mathrm{T}}(\alpha[A_2^0]^{\mathrm{T}} + [A_3^2]^{\mathrm{T}})[N]\,\mathrm{d}\xi \\
&\quad + \frac{\omega}{2}\int_{-1}^{1}[N]^{\mathrm{T}}(\alpha^2[A_4^0]^{\mathrm{T}} + \alpha[A_5^2]^{\mathrm{T}} + [A_6^2]^{\mathrm{T}})[N]\,\mathrm{d}\xi, \\
\boldsymbol{F}^2 &= \{\boldsymbol{a}_1^{\mathrm{T}}[N]^{\mathrm{T}}[B_4^1]^{\mathrm{T}}[N]\}|_{\theta=0,\omega} - \int_{-1}^{1}\boldsymbol{a}_1^{\mathrm{T}}[N']^{\mathrm{T}}[A_7^1]^{\mathrm{T}}[N]\,\mathrm{d}\xi - \frac{\omega}{2}\int_{-1}^{1}\boldsymbol{a}_1^{\mathrm{T}}[N]^{\mathrm{T}}(\alpha[A_8^1] + [A_9^2]^{\mathrm{T}})[N]\,\mathrm{d}\xi \\
&\quad - \frac{\omega}{2}\int_{-1}^{1}\boldsymbol{a}_0^{\mathrm{T}}[N]^{\mathrm{T}}[A_{10}^2]^{\mathrm{T}}[N]\,\mathrm{d}\xi.
\end{aligned} \tag{64}$$

For clamped boundary conditions $[B_2^0] = [B_3^2] = [B_4^1] = [0]$.

4.6. The non-uniqueness of $\boldsymbol{\varphi}_2, \boldsymbol{\psi}_2$ and the $\mathscr{H}_2$ condition

Similar to the $\boldsymbol{\varphi}_1$ solution, the differential equation describing $\boldsymbol{\varphi}_2$ and the differential equation describing $\boldsymbol{\psi}_2$ are both non-homogeneous. Thus

$$\boldsymbol{\varphi}_2(\theta) = \boldsymbol{\varphi}_2^{(P)}(\theta) + \boldsymbol{\varphi}_2^{(H)}(\theta), \quad \boldsymbol{\psi}_2(\theta) = \boldsymbol{\psi}_2^{(P)}(\theta) + \boldsymbol{\psi}_2^{(H)}(\theta) \tag{65}$$

Table 1
Numerical results of first three eigen-values and their relative error (%) for an isotropic ($\lambda = 0.5769, \mu = 0.3846$) cracked domain with traction free boundary conditions

p-level	DOF	$\alpha_1^{Ex} = 0.5$		$\alpha_2^{Ex} = 0.5$		$\alpha_3^{Ex} = 0.5$	
		α_1^{FE}	% Error	α_2^{FE}	% Error	α_3^{FE}	% Error
$p = 2$	18	–	–	–	–	0.551329	10.265780
$p = 3$	24	–	–	–	–	0.500139	0.027824
$p = 4$	30	0.577106	15.421192	0.899122	79.824361	0.500139	0.027824
$p = 5$	36	0.521094	4.218802	0.622920	24.584006	0.500000	0.000014
$p = 6$	42	0.507963	1.592520	0.517027	3.405338	0.500000	0.000014
$p = 7$	48	0.500843	0.168622	0.504260	0.851932	0.500000	0
$p = 8$	54	0.500162	0.032352	0.500281	0.056244	–	–
$p = 9$	60	0.500008	0.001532	0.500041	0.008206	–	–
$p = 10$	66	0.500001	0.000178	0.500001	0.000292	–	–
$p = 11$	72	0.500000	0.000004	0.500000	0.000028	–	–

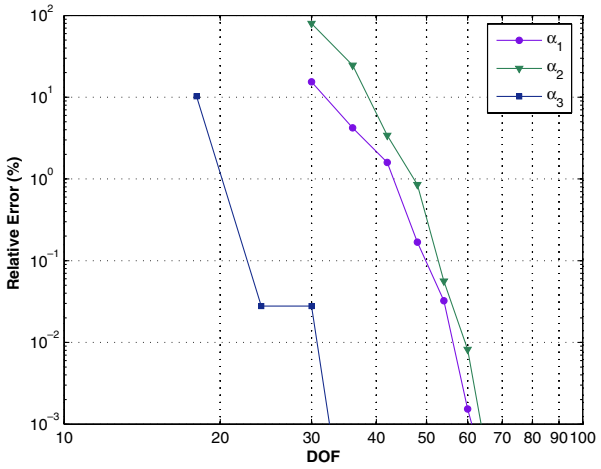

Fig. 2. Relative error of the eigen-values $\alpha_1^{\mathrm{FE}}, \alpha_2^{\mathrm{FE}}, \alpha_3^{\mathrm{FE}}$, for isotropic cracked domain with traction free boundary conditions ($\lambda = 0.5769, \mu = 0.3846$).

with

$$\boldsymbol{\varphi}_2^{(H)}(\theta) = C^{\varphi_2}\boldsymbol{\varphi}_0(\theta), \quad \boldsymbol{\psi}_2^{(H)}(\theta) = C^{\psi_2}\boldsymbol{\psi}_0(\theta). \tag{66}$$

Again C^{φ_2} and C^{ψ_2} are undefined, so any value of C^{φ_2} and C^{ψ_2}, including $C^{\varphi_2} = C^{\psi_2} = 0$ can be chosen. However, the shadow function $\boldsymbol{\varphi}_2$ and $\boldsymbol{\psi}_2$ have to satisfy another condition, denoted by $\mathscr{H}_2$ (for further details see [7]):

$$\begin{aligned}\mathscr{H}_2 = &\int_0^{\omega}\{\boldsymbol{T}_0^{\Gamma_R}\boldsymbol{\Phi}_2\cdot\boldsymbol{\Psi}_0 - \boldsymbol{\Phi}_2\cdot\boldsymbol{T}_0^{\Gamma_R}\boldsymbol{\Psi}_0\}\,\mathrm{d}\theta + \int_0^{\omega}\{\boldsymbol{T}_0^{\Gamma_R}\boldsymbol{\Phi}_0\cdot\boldsymbol{\Psi}_2 - \boldsymbol{\Phi}_0\cdot\boldsymbol{T}_0^{\Gamma_R}\boldsymbol{\Psi}_2\}\,\mathrm{d}\theta - \int_0^{\omega}\{\boldsymbol{T}_0^{\Gamma_R}\boldsymbol{\Phi}_1\cdot\boldsymbol{\Psi}_1 - \boldsymbol{\Phi}_1\cdot\boldsymbol{T}_0^{\Gamma_R}\boldsymbol{\Psi}_1\}\,\mathrm{d}\theta\\ &- \int_0^{\omega}\{\boldsymbol{T}_1^{\Gamma_R}\boldsymbol{\Phi}_0\cdot\boldsymbol{\Psi}_1 - \boldsymbol{\Phi}_0\cdot\boldsymbol{T}_1^{\Gamma_R}\boldsymbol{\Psi}_1\}\,\mathrm{d}\theta + \int_0^{\omega}\{\boldsymbol{T}_1^{\Gamma_R}\boldsymbol{\Phi}_1\cdot\boldsymbol{\Psi}_0 - \boldsymbol{\Phi}_1\cdot\boldsymbol{T}_1^{\Gamma_R}\boldsymbol{\Psi}_0\}\,\mathrm{d}\theta = 0,\end{aligned} \tag{67}$$

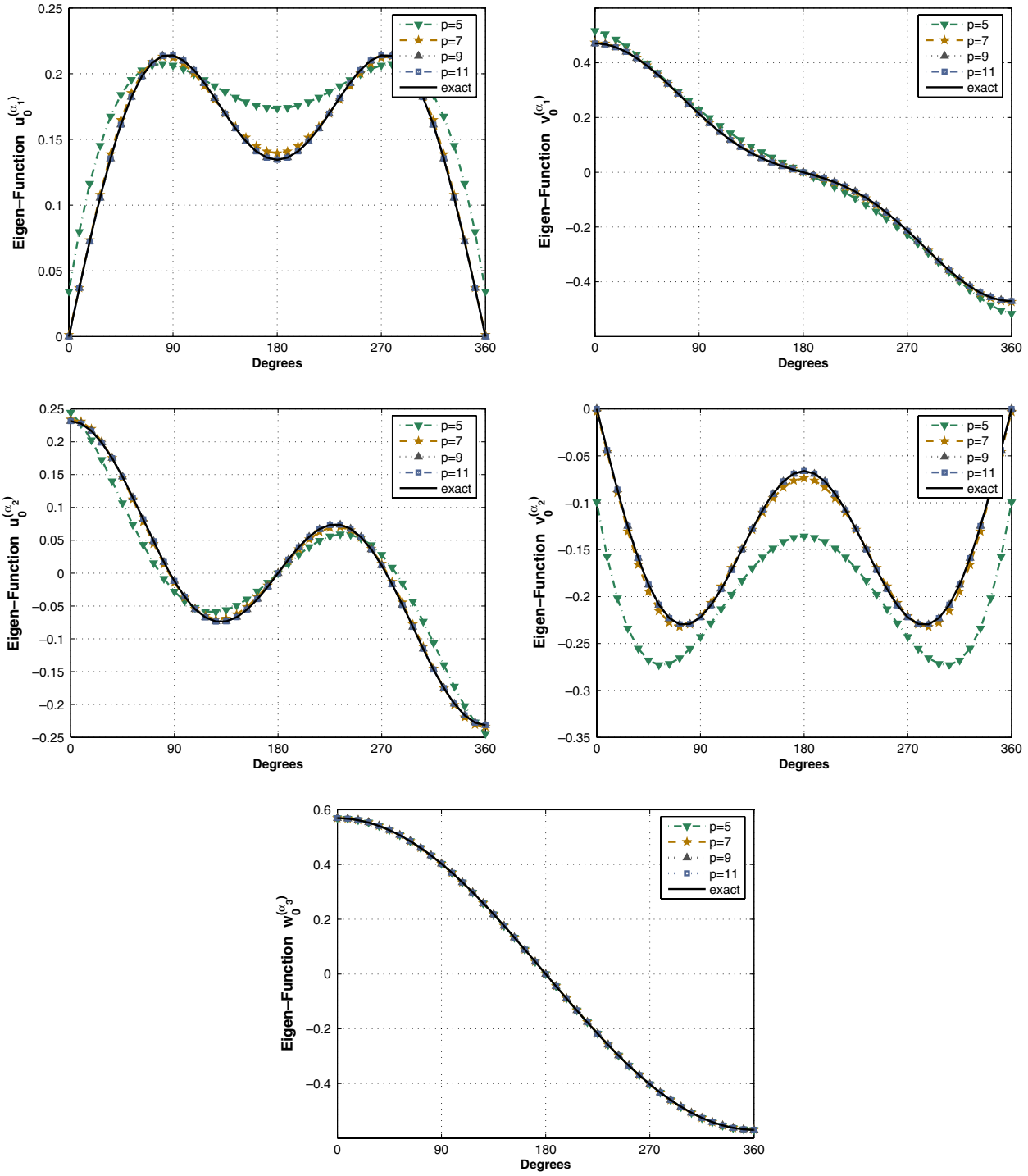

Fig. 3. Eigen-Functions $u_0^{(\alpha_i)}$ and $v_0^{(\alpha_i)}$ for $i = 1, 2$ and $w_0^{(\alpha_3)}$, for isotropic cracked domain with traction free boundary conditions ($\lambda = 0.5769, \mu = 0.3846$).

where $\boldsymbol{T}_0^{\Gamma_R}$ and $\boldsymbol{T}_1^{\Gamma_R}$ are given in (32). Once the functions $\boldsymbol{\varphi}_2$ and $\boldsymbol{\psi}_2$ are computed, $\mathscr{H}_2$ condition is computed. In the case $\mathscr{H}_2 \neq 0, \mathscr{H}_2$ is recomputed using

$$\boldsymbol{\psi}_2^{\mathrm{NEW}} = \boldsymbol{\psi}_2 + C^{\psi_2}\boldsymbol{\psi}_0. \tag{68}$$

The constant C^{ψ_2} is chosen such that $\mathscr{H}_2 = 0$.

5. Numerical example: Eigen-pairs and shadow function computation for cracked domain ($\omega = 2\pi$) with traction free boundary conditions

5.1. Primal eigen-pairs and duals, $\boldsymbol{\alpha}$, $\boldsymbol{\varphi}_0, \boldsymbol{\psi}_0$

In order to examine the method and its performance we first select an isotropic material for which we can compute $\boldsymbol{\varphi}_0$ analytically. The numerical results are compared with the analytical ones to assess the accuracy and efficiency of present methods.

We select Young modulus to be 1 and Poisson ration to be 0.3, so Lamé constants are $\lambda = 0.5769$ and $\mu = 0.3846$. The first three eigen-pairs are associated in fracture mechanics with Mode I, Mode II and Mode III deformations. The first three eigen-values for the case of cracked domain (computed analytically) are

$$\alpha_1^{Ex} = \alpha_2^{Ex} = \alpha_3^{Ex} = \frac{1}{2}. \tag{69}$$

The eigen-functions $\boldsymbol{\varphi}_0^{(\alpha_i)}$ associated with these three eigen-values and the duals $\boldsymbol{\psi}_0^{(\alpha_i)}$ are given in [22] and Appendix A.

Using a single finite element and increasing the order of shape functions, we summarize the eigen-values, relative error, p-level and the number of degrees of freedom in Table 1. The exponential rate of convergence of the eigen-values as expected for p-extensions is clearly visible when plotted on a log–log scale in Fig. 2.

The eigen-functions u_0, v_0 associated with α_1, α_2 and w_0 for α_3 are presented in Fig. 3. The function w_0 associated with α_1 and α_2 is zero and therefore not plotted herein as well as u_0 and v_0 for α_3.

Defining the relative error in L^2 norm for u_0, for example, by

$$\|e(u_0)\|_{L^2} = \frac{\int_0^{\omega}(u_0^{\mathrm{FE}} - u_0^{Ex})^2\,\mathrm{d}\theta}{\int_0^{\omega}(u_0^{Ex})^2\,\mathrm{d}\theta}, \tag{70}$$

we plot the relative errors for $u_0^{(\alpha_1)}, v_0^{(\alpha_1)}, u_0^{(\alpha_2)}, v_0^{(\alpha_2)}$ and $w_0^{(\alpha_3)}$ in Fig. 4. As expected, exponential convergence rate is noticed.

The dual eigen-functions u_0, v_0 associated with $-\alpha_1, -\alpha_2$ and w_0 for $-\alpha_3$ are presented in Fig. 5. The functions w_0 associated with $-\alpha_1$ and $-\alpha_2$ is zero and therefore not plotted herein as well as u_0 and v_0 associated with $-\alpha_3$.

We plot the relative errors for the duals $u_0^{(-\alpha_1)}, v_0^{(-\alpha_1)}, u_0^{(-\alpha_2)}, v_0^{(-\alpha_2)}$ and $w_0^{(-\alpha_3)}$ in Fig. 6. The duals show also an exponential convergence rate.

5.2. Computation of the first primal and dual shadow functions, $\boldsymbol{\varphi}_1$ and $\boldsymbol{\psi}_1$

There are many valid $\boldsymbol{\varphi}_1$ and $\boldsymbol{\psi}_1$ functions (see Section 4.3) so that we cannot compare them with the analytical solution. In Fig. 7 the first shadow functions and the first dual shadow functions associated with $\alpha_1, \alpha_2, \alpha_3$ computed by (47) with $p = 11$ are shown.

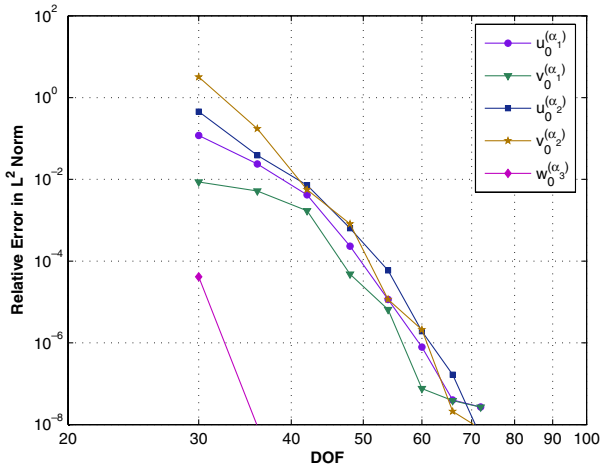

Fig. 4. Relative error in L^2 norm for the eigen-functions $u_0^{(\alpha_i)}$ and $v_0^{(\alpha_i)}$ for $i = 1, 2$ and $w_0^{(\alpha_3)}$, for isotropic cracked domain with traction free boundary conditions ($\lambda = 0.5769, \mu = 0.3846$).

5.3. Computation of the second primal and dual shadow functions, φ_2 and ψ_2

There are many valid φ_2 and ψ_2 functions and therefore we cannot compare them with the analytical solution. The second shadow functions and the second dual shadow functions associated with α_1, α_2 and α_3 computed by (63) with $p = 11$ are shown in Fig. 8. These will be used in the sequel for the extraction of the edge stress intensity functions.

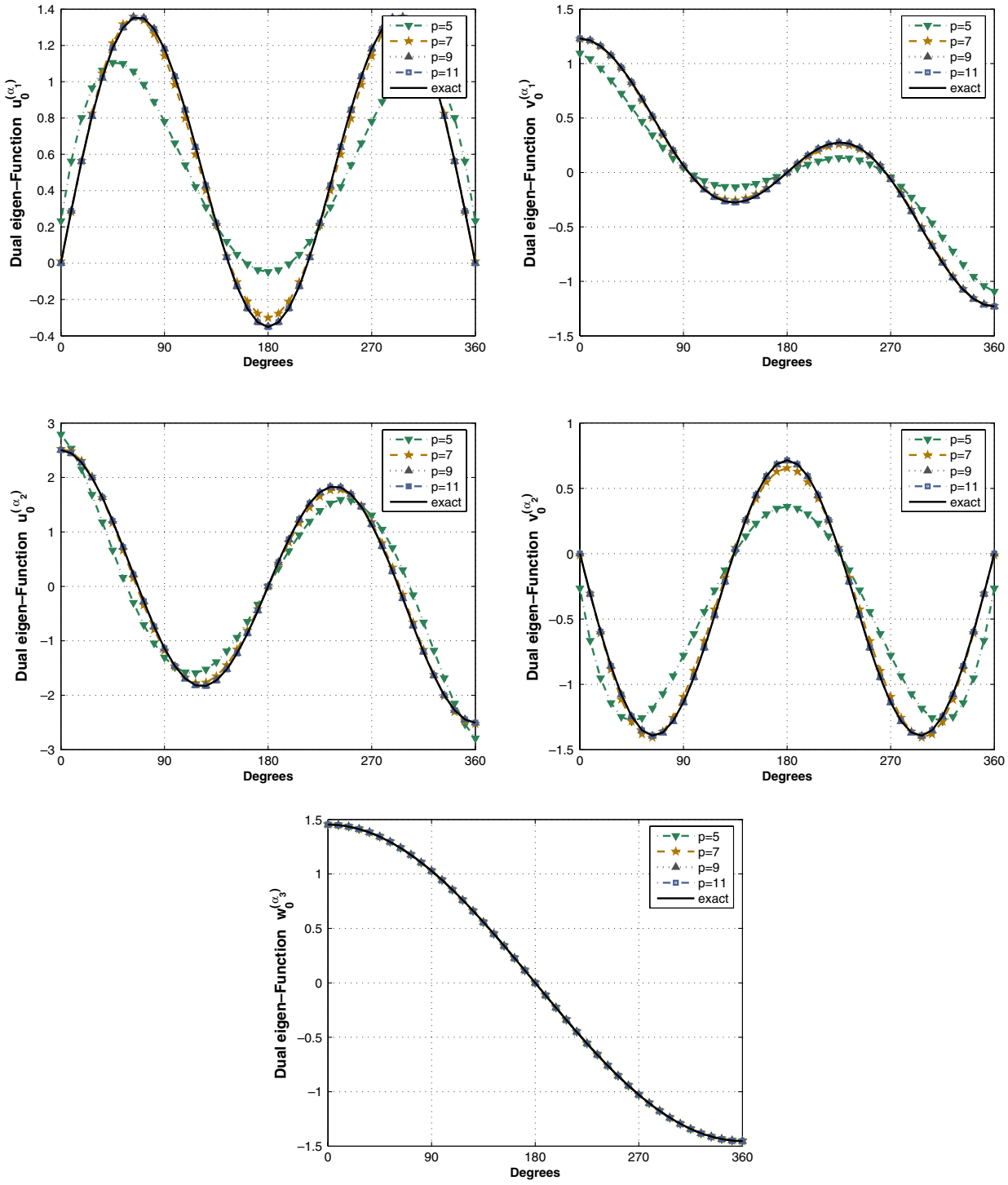

Fig. 5. Dual eigen-Functions $u_0^{(-\alpha_i)}$ and $v_0^{(-\alpha_i)}$ for $i = 1, 2$ and $w_0^{(-\alpha_3)}$, for isotropic cracked domain with traction free boundary conditions ($\lambda = 0.5769, \mu = 0.3846$).

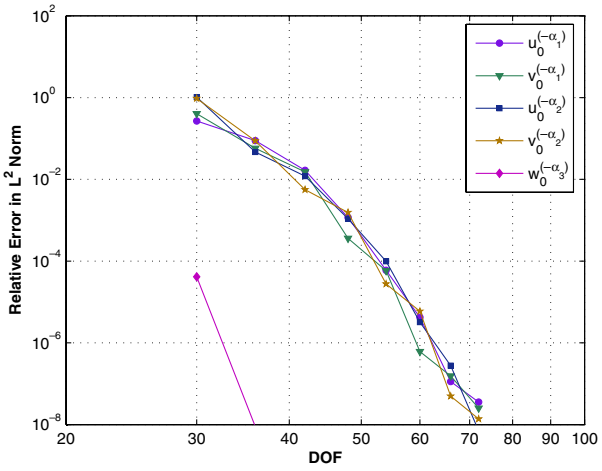

Fig. 6. Relative error in L^2 norm for the dual eigen-functions $u_0^{(-\alpha_i)}$ and $v_0^{(-\alpha_i)}$ for $i = 1, 2$ and $w_0^{(-\alpha_3)}$, for isotropic cracked domain with traction free boundary conditions ($\lambda = 0.5769, \mu = 0.3846$).

6. Extracting edge stress intensity function by the quasi-dual function method

Following the computation of the asymptotic series representing the elastic solution in the vicinity of an edge, we proceed to extraction of edge stress intensity functions by using the quasi-dual function method [7]. This extraction method has been presented for scalar elliptic problems in [16] and for elastic *isotropic* problems in [22]. Herein we demonstrate its efficiency when the eigen-pairs and the shadow functions are computed numerically for a general anisotropic domain. We briefly describe herein the quasi-dual function method, whereas full details are given in [7,16,22].

Assume that the edge stress intensity function (ESIF) $A_i(x_3)$ is of interest. For its extraction a *quasi-dual*-singular function $\mathbf{K}_m^{(\alpha_i)}[B]$ is constructed where m is a natural integer called the *order* of the quasi-dual function, and $B(x_3)$ is a function, provided in the sequel, called *extraction polynomial*. $\mathbf{K}_m^{(\alpha_i)}[B]$ is characterized by the number of dual singular functions m needed to construct it and the extraction polynomial B:

$$\mathbf{K}_m^{(\alpha_i)}[B] \stackrel{\text{def}}{=} \sum_{j=0}^{m} \partial_3^j B(x_3) \boldsymbol{\Psi}_j^{(\alpha_i)}. \tag{71}$$

A scalar product of $A_i(x_3)$ with $B(x_3)$ on $\mathscr{E}$ can be extracted with the help of the *anti-symmetric* boundary integral $J[R]$, over the cylindrical surface Γ_R (1).

$$J[R](\mathbf{f}, \boldsymbol{v}) \stackrel{\text{def}}{=} \int_I \int_0^{\omega} (\boldsymbol{T}^{\Gamma_R}\mathbf{f} \cdot \boldsymbol{v} - \mathbf{f} \cdot \boldsymbol{T}^{\Gamma_R}\boldsymbol{v})|_{r=R} R \,\mathrm{d}\theta \,\mathrm{d}x_3, \tag{72}$$

where $I \equiv \mathscr{E}$ (the edge) along x_3 axis (Fig. 1) and $\boldsymbol{T}^{\Gamma_R}$ is the radial Neumann trace operator presented in (30). Note that $J[R]$ in (72) is unrelated with the classical J-integral [17], but rather an extension of the dual singular function method [3] to 3-D domains. With the above definitions we have the following theorem [7]:

Theorem 1. *Take $B(x_3)$ such that*

$$\partial_3^j B(x_3) = 0 \quad \text{for } j = 0, \ldots, m-1 \text{ on } \partial I \tag{73}$$

then, if the ESIFs A_i in the expansion (7) are smooth enough:

$$J[R](\tilde{\boldsymbol{u}}, \mathbf{K}_m^{(\alpha_i)}[B]) = \int_I A_i(x_3) B(x_3) \,\mathrm{d}x_3 + \mathscr{O}(R^{\alpha_1 - \alpha_i + m + 1}), \quad \text{as } R \to 0. \tag{74}$$

Here α_1 is the smallest of the positive real eigen-values $\alpha_i, i \in \mathbb{N}$, and we assume that any other complex eigen-value α with positive real part satisfies $\Re\alpha \geqslant \alpha_1$, as mentioned in Remark 2.

Choosing $m = 2$ we have in (74) $\mathscr{O}(R^{\alpha_1 - \alpha_i + 3})$. Theorem 1 allows a precise determination of $\int_I A_i(x_3)B(x_3)\,\mathrm{d}x_3$ by computing (74) for two or three R values as $R \to 0$. We construct an adaptive class of orthonormal polynomials (Jacobi) with a given weight $w(x_3) = (1 - x_3^2)^{\tilde{m}}$ so to represent $B(x_3)$. In this way, if $A_i(x_3)$ is a polynomial of degree N, it is expanded as a linear

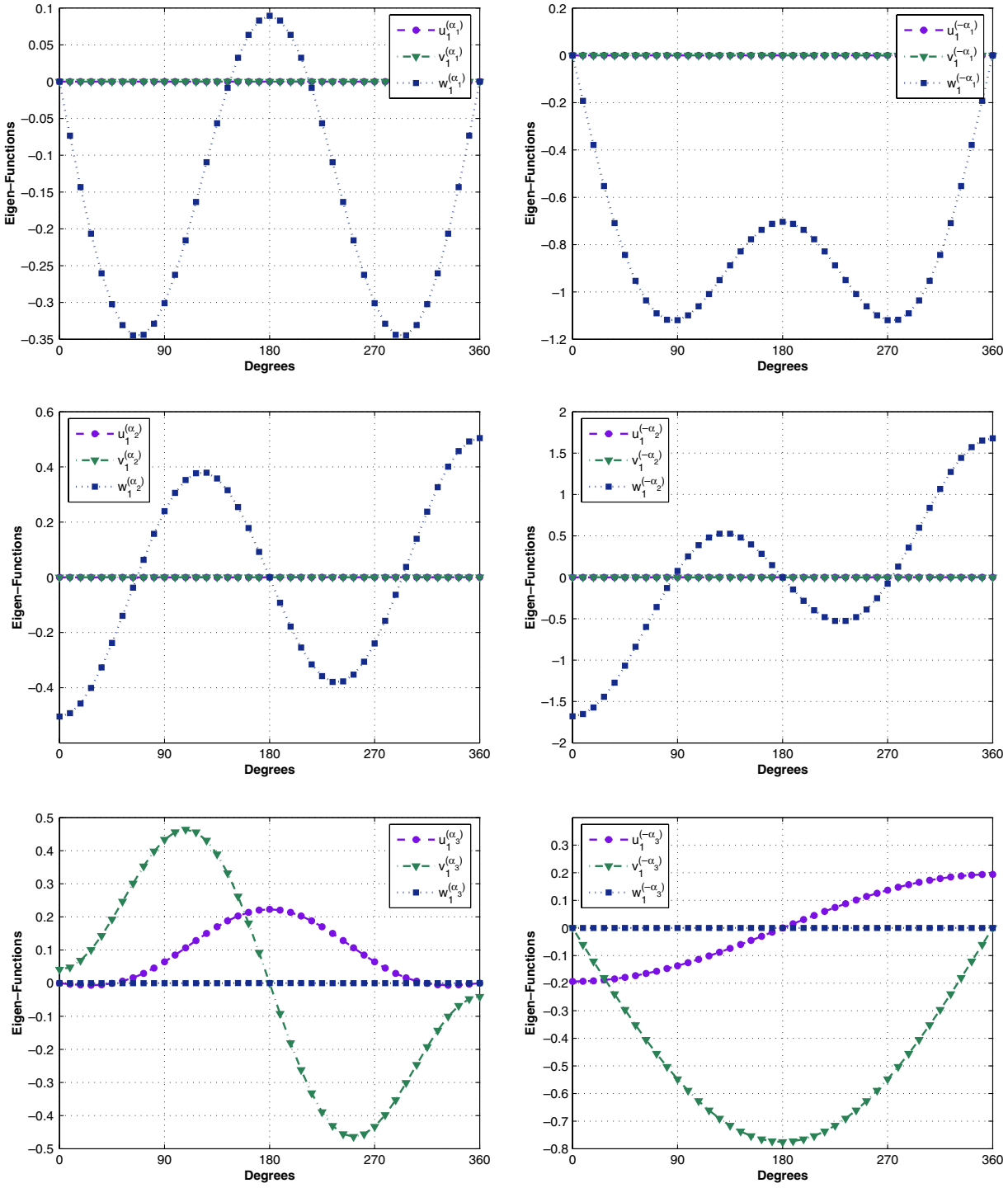

Fig. 7. First shadow function $\boldsymbol{\varphi}_1$ (left) and dual shadow function $\boldsymbol{\psi}_1$ (right) associated with α_1 (Mode I) first row, α_2 (Mode II) second row, and α_3 (Mode III) third row, for isotropic cracked domain with traction free boundary conditions ($\lambda = 0.5769, \mu = 0.3846$) using $p = 11$.

combination of Jacobi polynomials. By selecting $\tilde{m} = m = 2$, (73) is satisfied, however the derivatives of these Jacobi polynomials are significantly large which effect the result of the extracted ESIF at the two ends of the edge (see [22]). Therefore we choose $\tilde{m} = 4$ which satisfy (73) up to $m = 4$. The family of extraction polynomials is

$$B^{(k)}(x_3) = (1 - x_3^2)^4 \frac{J_4^{(k)}(x_3)}{h_k}, \quad h_k = \frac{2^9(k+4)!(k+4)!}{(2k+9)(k+8)!}. \tag{75}$$

If $A_i(x_3)$ is represented by a polynomial of Nth order as linear combination of Jacobi polynomials,

$$A_i(x_3) = \tilde{a}_0 J_4^{(0)} + \tilde{a}_1 J_4^{(1)}(x_3) + \cdots + \tilde{a}_N J_4^{(N)}(x_3), \tag{76}$$

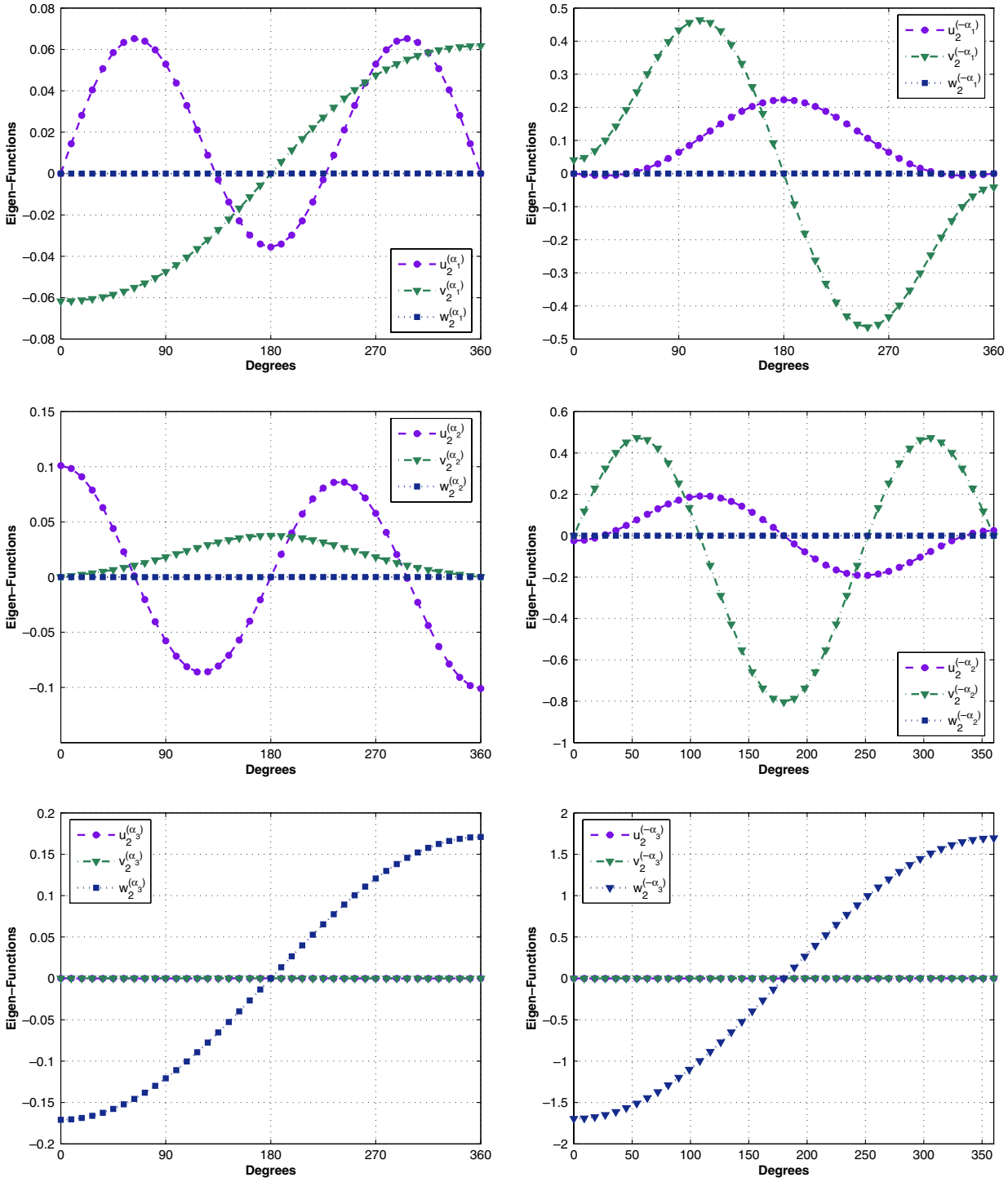

Fig. 8. Second shadow function $\boldsymbol{\varphi}_2$ (left) and dual shadow function $\boldsymbol{\psi}_2$ (right) associated with α_1 (Mode I) first row, α_2 (Mode II) second row, and α_3 (Mode III) third row, for isotropic cracked domain with traction free boundary conditions ($\lambda = 0.5769, \mu = 0.3846$) using $p = 11$.

where $J_4^{(k)}$ is the Jacobi polynomial of degree k and order 4 then

$$\int_{-1}^{1} A_i(x_3) B^{(k)}(x_3)\,\mathrm{d}x_3 = \tilde{a}_k \quad k = 0, 1, \ldots, N. \tag{77}$$

Thus, in the view of (74), the $J[R]$ integral evaluated for the quasi-dual functions $K_m^{(\alpha_i)}[B^{(k)}]$, $k = 0, 1, \ldots, N$ provides approximations of the coefficients $\tilde{a}_k$. Note that the polynomial degree is the superscript k. Of course, in general $A_i(x_3)$ is an

unknown function and we wish to find a projection of it into spaces of polynomials. It is expected that as we increase the polynomial space, the approximation is better.

If we want to increase the space in which $A_i(x_3)$ is projected, all which is needed is the computation of (74) for $k = N+1$. This way: $A^{\text{new}}(x_3) = A^{\text{previous}}(x_3) + \tilde{a}_{N+1}J_{N+1}(x_3)$.

In a cracked domain subject to boundary conditions the exact solution $\tilde{\boldsymbol{u}}$ is in general unknown, so we have to use finite element methods and obtain $\tilde{\boldsymbol{u}}_{\text{FE}}$ instead, to be used in (72), and computed using a Gaussian quadrature of order n_G:

$$J[R](\tilde{\boldsymbol{u}}, \mathbf{K}_2^{(\alpha_i)}[B^{(k)}]) = \sum_{k=1}^{n_G}\sum_{\ell=1}^{n_G}\frac{\omega}{2}w_k w_\ell(\boldsymbol{T}^{\Gamma_R}\tilde{\boldsymbol{u}}_{\text{FE}}\cdot\mathbf{K}_2^{(\alpha_i)}[B^{(k)}] - \tilde{\boldsymbol{u}}_{\text{FE}}\cdot\boldsymbol{T}^{\Gamma_R}\mathbf{K}_2^{(\alpha_i)}[B^{(k)}])_{\xi_k,\eta_\ell}, \tag{78}$$

where w_k are the weights and ξ_k and η_ℓ are the abscissas of the Gaussian quadrature. The Neumann trace operator, $\boldsymbol{T}^{\Gamma_R}$, operates on both $\tilde{\boldsymbol{u}}_{\text{FE}}$ and $\mathbf{K}_2^{(\alpha_i)}[B^{(k)}]$. For $\tilde{\boldsymbol{u}}_{\text{FE}}$ and $\boldsymbol{T}^{\Gamma_R}\tilde{\boldsymbol{u}}_{\text{FE}}$ we use the numerical approximations computed by finite elements (notice that such extractions are easily computed by the p-version of the FEM at any point within an element), whereas $\mathbf{K}_2^{(\alpha_i)}[B^{(k)}]$ and $\boldsymbol{T}^{\Gamma_R}\mathbf{K}_2^{(\alpha_i)}[B^{(k)}]$ are computed numerically using $\boldsymbol{\psi}_0^{\text{FE}}, \boldsymbol{\psi}_1^{\text{FE}}$ and $\boldsymbol{\psi}_2^{\text{FE}}$ in Sections 3 and 4.

6.1. Numerical example: ESIFs extraction for an isotropic cracked domain ($\omega = 2\pi$) with traction free boundary conditions

The extraction method of the ESIFs for isotropic domains was presented in [22]. It was shown to be accurate and efficient, however, the available dual eigen-pairs and shadow functions were all analytical. In this subsection we examine the extraction method using $\boldsymbol{\Psi}_0^{\text{FE}}, \boldsymbol{\Psi}_1^{\text{FE}}, \boldsymbol{\Psi}_2^{\text{FE}}$ computed numerically. We choose the Young modulus to be 1 and Poisson ratio 0.3, ($\lambda = 0.5769$ and $\mu = 0.3846$), so

$$\mathbf{C} = \begin{pmatrix} 1.346153 & 0.576923 & 0.576923 & 0 & 0 & 0 \\ & 1.346153 & 0.576923 & 0 & 0 & 0 \\ & & 1.346153 & 0 & 0 & 0 \\ & & & 0.384615 & 0 & 0 \\ & & & & 0.384615 & 0 \\ & & & & & 0.384615 \end{pmatrix}. \tag{79}$$

Having the exact solution to a crack in a 3-D isotropic domain with traction free boundary conditions we can consider the first three eigen-values only, and chose the ESIFs to be, for example, a polynomial of order 3. Thus an exact solution is

$$\begin{aligned}\tilde{\boldsymbol{u}} = {} & A_1(x_3)r^{\alpha_1}\boldsymbol{\varphi}_0^{(\alpha_1)}(\theta) + \partial_3 A_1(x_3)r^{\alpha_1+1}\boldsymbol{\varphi}_1^{(\alpha_1)}(\theta) + \partial_3^2 A_1(x_3)r^{\alpha_1+2}\boldsymbol{\varphi}_2^{(\alpha_1)}(\theta) + A_2(x_3)r^{\alpha_2}\boldsymbol{\varphi}_0^{(\alpha_2)}(\theta) + \partial_3 A_2(x_3)r^{\alpha_2+1}\boldsymbol{\varphi}_1^{(\alpha_2)}(\theta) \\ & + \partial_3^2 A_2(x_3)r^{\alpha_2+2}\boldsymbol{\varphi}_2^{(\alpha_2)}(\theta) + A_3(x_3)r^{\alpha_3}\boldsymbol{\varphi}_0^{(\alpha_3)}(\theta) + \partial_3 A_3(x_3)r^{\alpha_3+1}\boldsymbol{\varphi}_1^{(\alpha_3)}(\theta) + \partial_3^2 A_3(x_3)r^{\alpha_3+2}\boldsymbol{\varphi}_2^{(\alpha_3)}(\theta),\end{aligned} \tag{80}$$

where all eigen-pairs and shadows in (80) are given analytically in Appendix A. For example, consider the following exact ESIFs (polynomials of order 3):

$$A_1^{Ex}(x_3) = 3 + 4x_3 + 5x_3^2, \quad A_2^{Ex}(x_3) = 2 + 3x_3 + 4x_3^2, \quad A_3^{Ex}(x_3) = 5 + 4x_3 + 2x_3^2. \tag{81}$$

If we prescribe on a traction free cracked domain Dirichlet boundary conditions according to (80) and (81), the exact solution at each r, θ, x_3 is as (80) and (81). Consider a 3-D domain as shown in Fig. 1 with $\omega = 2\pi$. The domain is discretized by using a p-FEM mesh, with geometrical progression towards the singular edge with a factor of 0.15, having four layers of elements. In the x_3 direction, a uniform discretization using five elements has been adopted. In Fig. 9 we present the mesh used for the cracked domain.

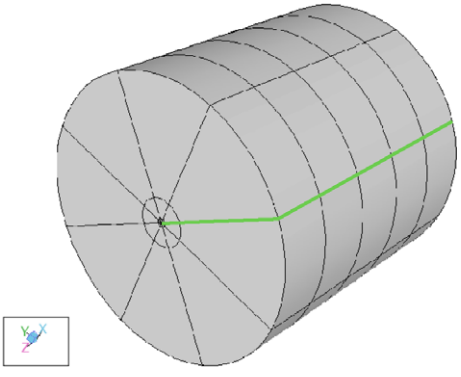

Fig. 9. The p-FEM model of the cracked domain.

We specify on the entire boundary $\partial\Omega$ Dirichlet boundary conditions according to the exact solution $\tilde{\boldsymbol{u}}$ (80). This way, the exact solution at any point $\boldsymbol{x} \equiv (r, \theta, x_3)$ is (80).

When $J[R]$ is computed with the quasi-dual function $\mathbf{K}_2^{(\alpha_i)}$ and $B^{(k)}(x_3)$ we expect to obtain, according to (74), the coefficient $\tilde{a}_j^{(\alpha_i)}$. The ESIF is then easily represented by a linear combination of the Jacobi polynomials in (76): We extract the ESIFs at $R = 0.05$ by using the *numerically computed* dual eigen-pairs and their shadows for construction of $K_2^{(\alpha_i)}[B^{(k)}]$.

We compute the relative error of the extracted $A_1^{\mathrm{FE}}(x_3), A_2^{\mathrm{FE}}(x_3), A_3^{\mathrm{FE}}(x_3)$ of order $3,4,5$ in Fig. 10. We compare these results with the extracted polynomial representation obtained using analytical formulas of the duals and shadows (see [22] for further details).

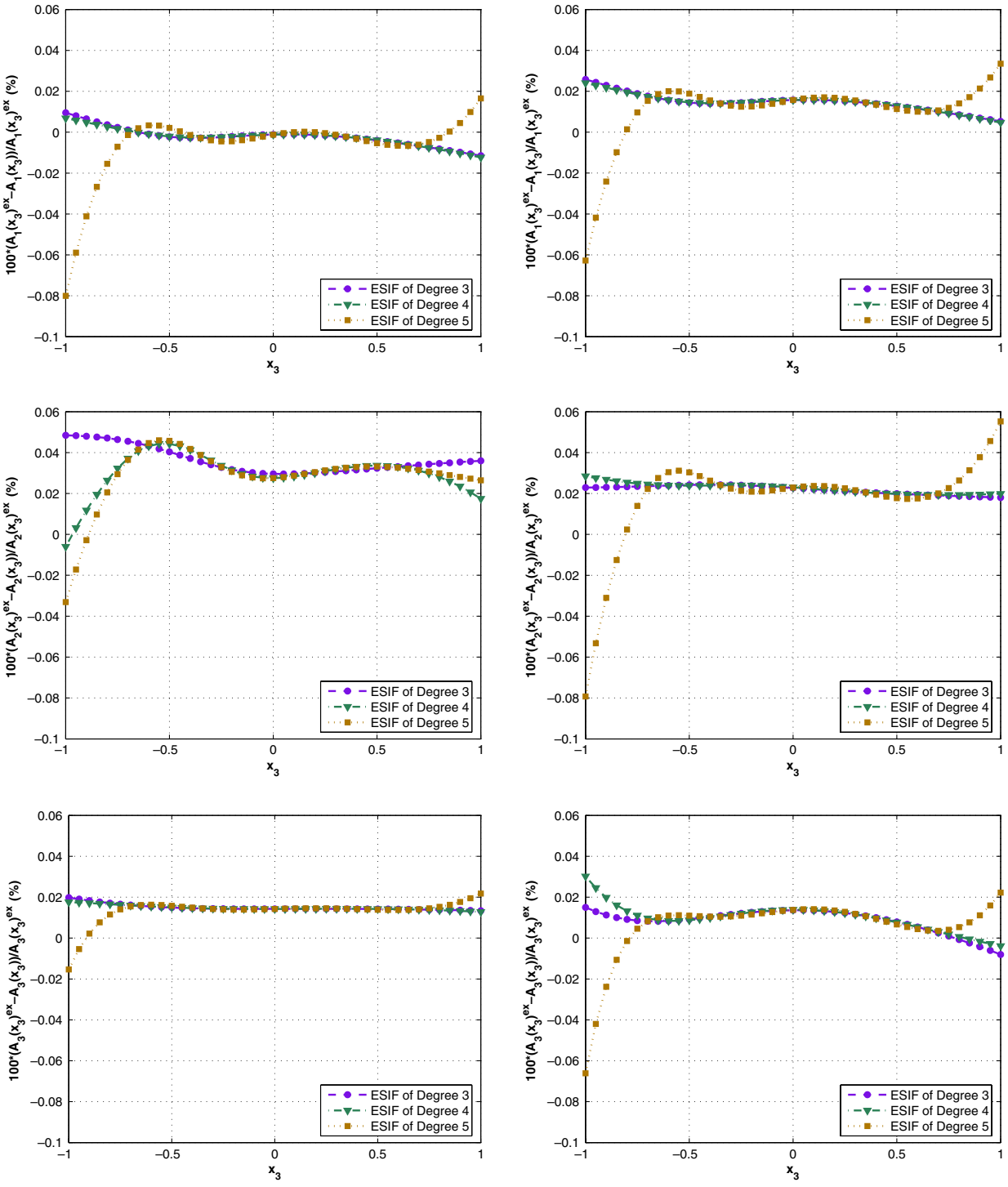

Fig. 10. Relative error of ESIFs computed using analytical (left) and numerical p-FEM (right) duals and shadows. Computation done with $B^{(k)}, k = 3, 4, 5$, where $A_1^{Ex}(x_3) = 3 + 4x_3 + 5x_3^2$, $A_2^{Ex}(x_3) = 2 + 3x_3 + 4x_3^2$, $A_3^{Ex}(x_3) = 5 + 4x_3 + 2x_3^2$, $\omega = 2\pi$, $\lambda = 0.5769$ and $\mu = 0.3846$, at $R = 0.05$.

Notice that the relative error of both ESIFs computed using either analytical or numerical dual and shadows functions are similar and in all cases lower than 0.1%. The results are accurate and efficient.

The same test was performed for a clamped V-notched domain $\left(\omega = \frac{3\pi}{2}\right)$. The ESIFs were extracted using numerically computed duals and shadows and the results compared to the ESIFs extracted using analytic computations of these functions. The results obtained were accurate, showing that both cases provide relative errors of less than 0.1%.

6.2. Numerical example: ESIFs extraction for an anisotropic cracked domain ($\omega = 2\pi$) with traction free boundary conditions

In this section we present the solution of the displacements in the vicinity of an edge for a traction free cracked anisotropic domain. The computation of the eigen-pairs, duals and shadows for anisotropic domain is not documented in the literature (to the best of our knowledge). We generate the solution in the vicinity of the edge using the numerically computed eigen-pairs and shadows and test the ESIF extraction method for the anisotropic domain.

We select the material *anisotropic* matrix to be (notice that $C_{23} = C_{12} \neq C_{13}$)

$$\mathbf{C} = \begin{pmatrix} 1.346153 & 0.576923 & 1.153846 & 0 & 0 & 0 \\ & 1.346153 & 0.576923 & 0 & 0 & 0 \\ & & 1.346153 & 0 & 0 & 0 \\ & & & 0.384615 & 0 & 0 \\ & & & & 0.384615 & 0 \\ & & & & & 0.384615 \end{pmatrix}. \tag{82}$$

Herein, we use the $\mathbf{C}$ matrix in a Cartesian Hooke's Law: $\boldsymbol{\sigma} = \mathbf{C}\boldsymbol{\varepsilon}$.

Remark 5. Computation of eigen-pairs and shadows in the case of a Cartesian Hook's law is similar to the method presented in Sections 3 and 4. By transferring the stresses $\boldsymbol{\sigma}$ and strains $\boldsymbol{\varepsilon}$ to Polar coordinate system $(\tilde{\boldsymbol{\sigma}}, \tilde{\boldsymbol{\varepsilon}})$ the material matrix $\mathbf{C}$ becomes θ dependent and therefore the $[A_i^j]$ and $[B_i^j]$ matrices are also θ dependent, however the method remains the same.

For anisotropic materials $\boldsymbol{\Phi}_0, \boldsymbol{\Phi}_1, \boldsymbol{\Phi}_2$ as well as $\boldsymbol{\Psi}_0, \boldsymbol{\Psi}_1, \boldsymbol{\Psi}_2$, are unknown, but the first three eigen-values for a cracked domain $(\omega = 2\pi)$ are $\alpha_1^{Ex} = \alpha_2^{Ex} = \alpha_3^{Ex} = \frac{1}{2}$ (for general elliptic systems with the same boundary conditions on both sides of crack faces, the first three singularity exponents are $\frac{1}{2}$, see [5]).

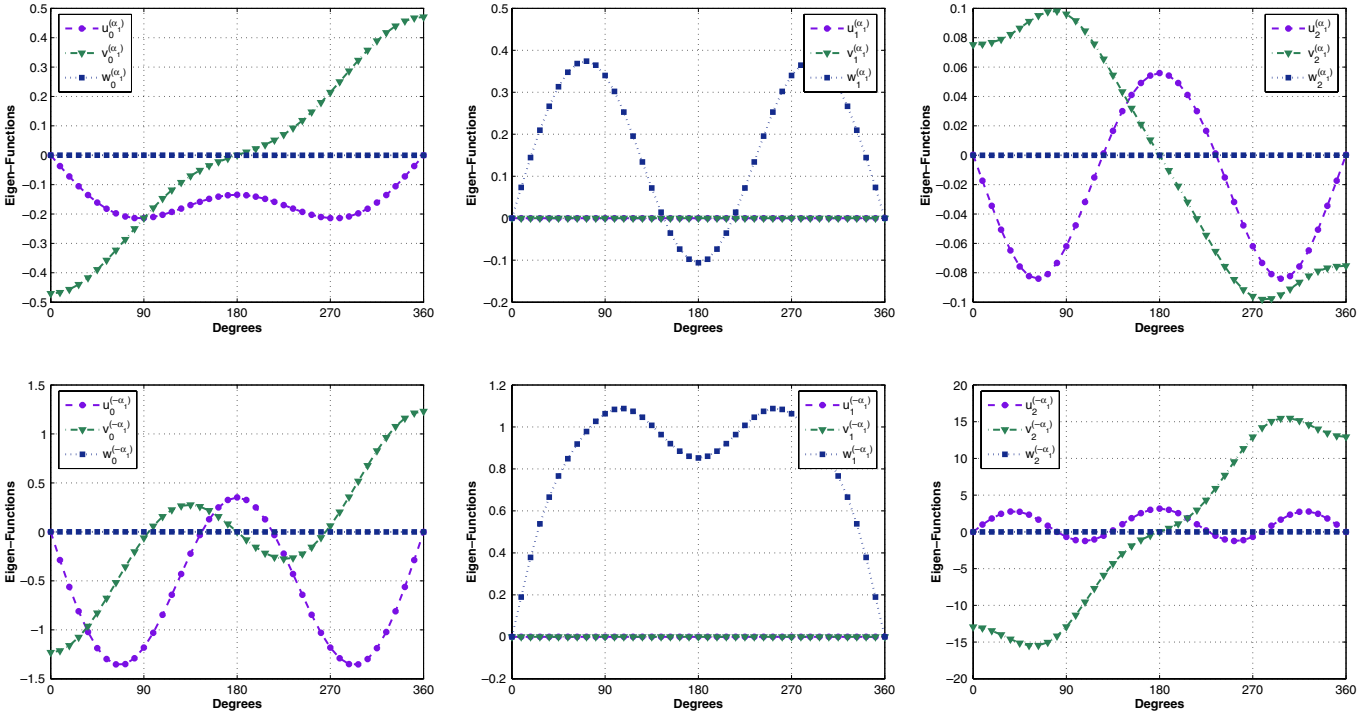

Fig. 11. The eigen-functions (top) and the dual eigen-functions (bottom) associated with $\alpha_1 = \frac{1}{2}$ in the case of anisotropic (82) cracked domain.

We first compute numerically the first three eigen-values as in Section 3. The eigen-values, relative error, p-level and the number of degrees of freedom are identical to these presented in Table 1 and therefore are not repeated. Although the eigen-values for the anisotropic case are identical to these of the isotropic case, the shadow functions of the two cases are different.

The primal, dual and shadow functions related with α_1, α_2 and α_3 are presented in Figs. 11–13, respectively. All functions presented herein were computed numerically at $p = 11$.

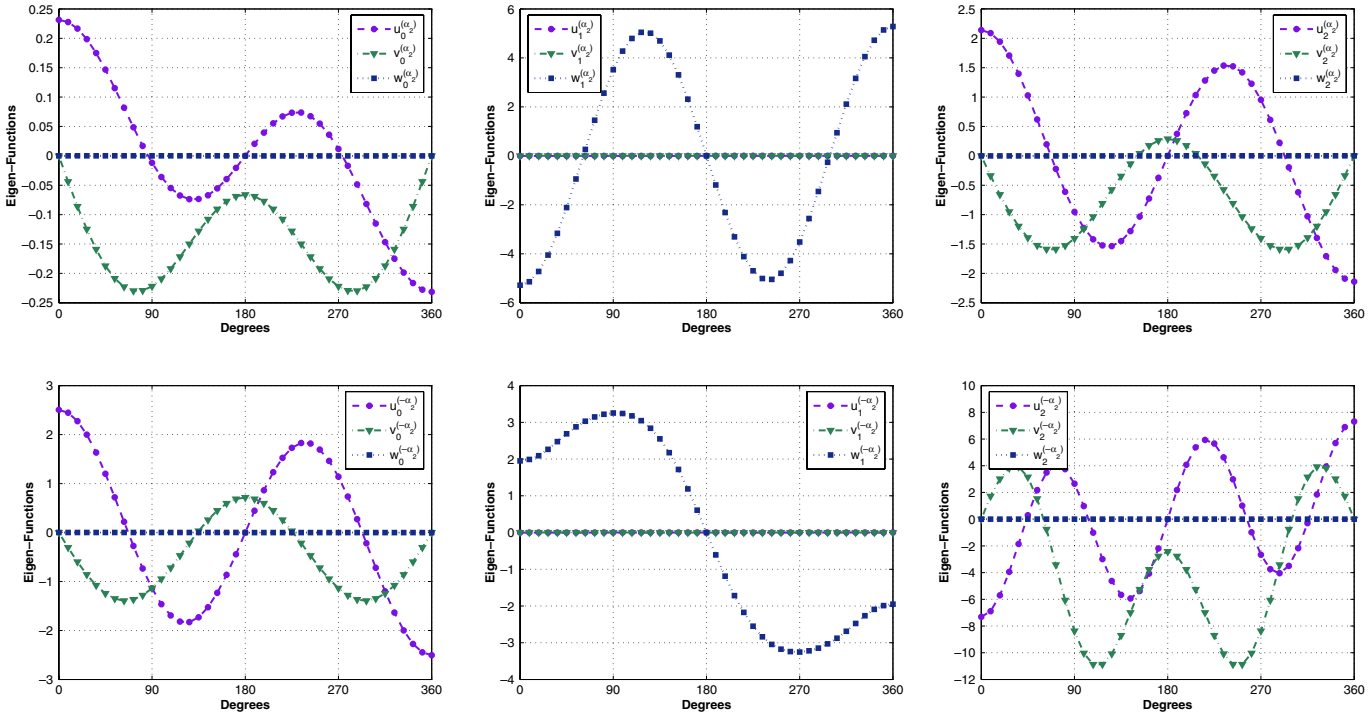

Fig. 12. The eigen-functions (top) and the dual eigen-functions (bottom) associated with $\alpha_2 = \frac{1}{2}$ in the case of anisotropic (82) cracked domain.

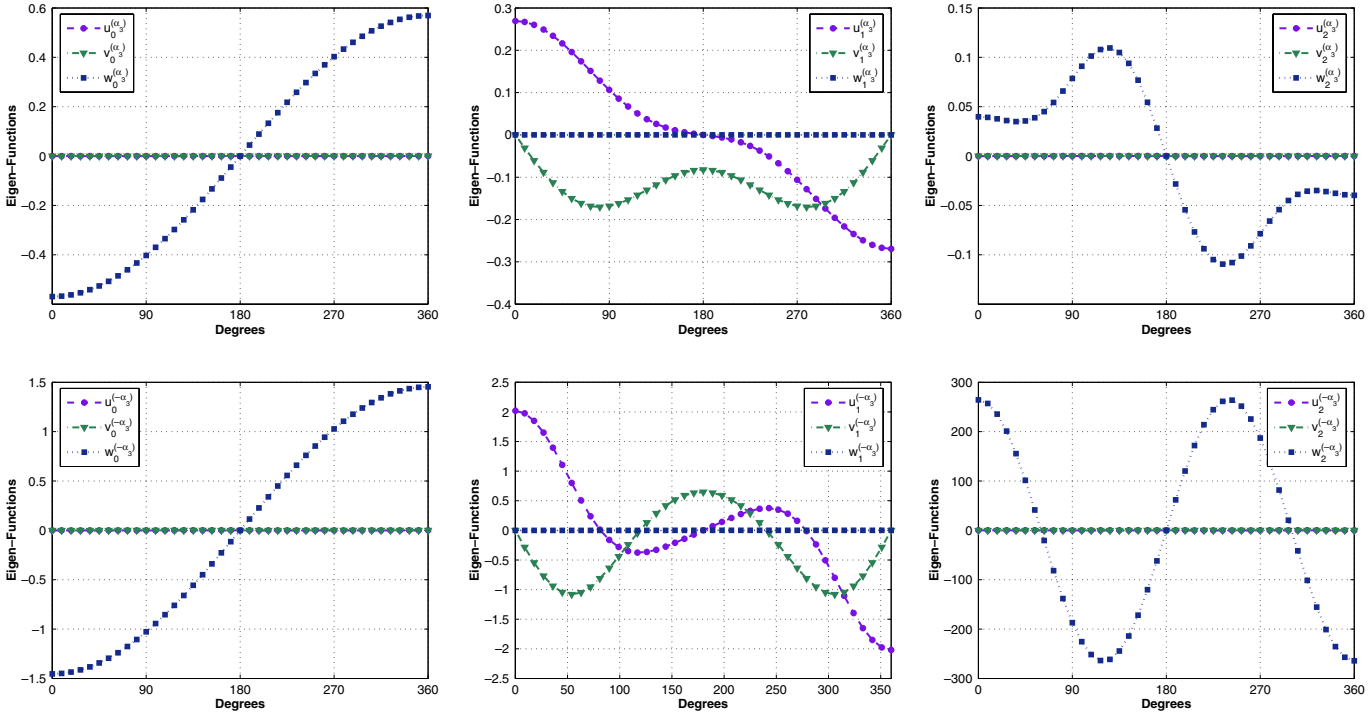

Fig. 13. The eigen-functions (top) and the dual eigen-functions (bottom) associated with $\alpha_3 = \frac{1}{2}$ in the case of anisotropic (82) cracked domain.

Similar to Section 6.1, we generate a solution to a crack in a three-dimensional anisotropic domain with traction free boundary conditions by applying the primal and shadow eigen-functions $\boldsymbol{\Phi}_0^{\mathrm{FE}}, \boldsymbol{\Phi}_1^{\mathrm{FE}}, \boldsymbol{\Phi}_2^{\mathrm{FE}}$ (we refer to the first three eigen-values only) computed at $p = 11$. We select the ESIF $A_i(x_3)$ to be polynomials of order 2 as presented in (81), such that the solution (7) contains nine terms in the sum: three eigen-functions and six shadow functions, as in (80). Because an analytical solution is unavailable we have to subscribe $\boldsymbol{\Phi}_0^{\mathrm{FE}}, \boldsymbol{\Phi}_1^{\mathrm{FE}}$ and $\boldsymbol{\Phi}_2^{\mathrm{FE}}$ instead as boundary conditions.

The domain has been discretized by using p-FEM mesh, as presented in Fig. 9. We specify on the entire boundary $\partial\Omega$ Dirichlet boundary conditions. This way, the solution at any point $\boldsymbol{x} \equiv (r, \theta, x_3)$ is as in (80).

We compute the polynomial that approximates the ESIFs using the $J[R]$ integrals with $K_2^{(\alpha_i)}$ at $R = 0.05$, and Jacobi polynomials of order 3,4 and 5, and plot $A_1^{\mathrm{FE}}(x_3), A_2^{\mathrm{FE}}(x_3), A_3^{\mathrm{FE}}(x_3)$ and their relative errors in Fig. 14.

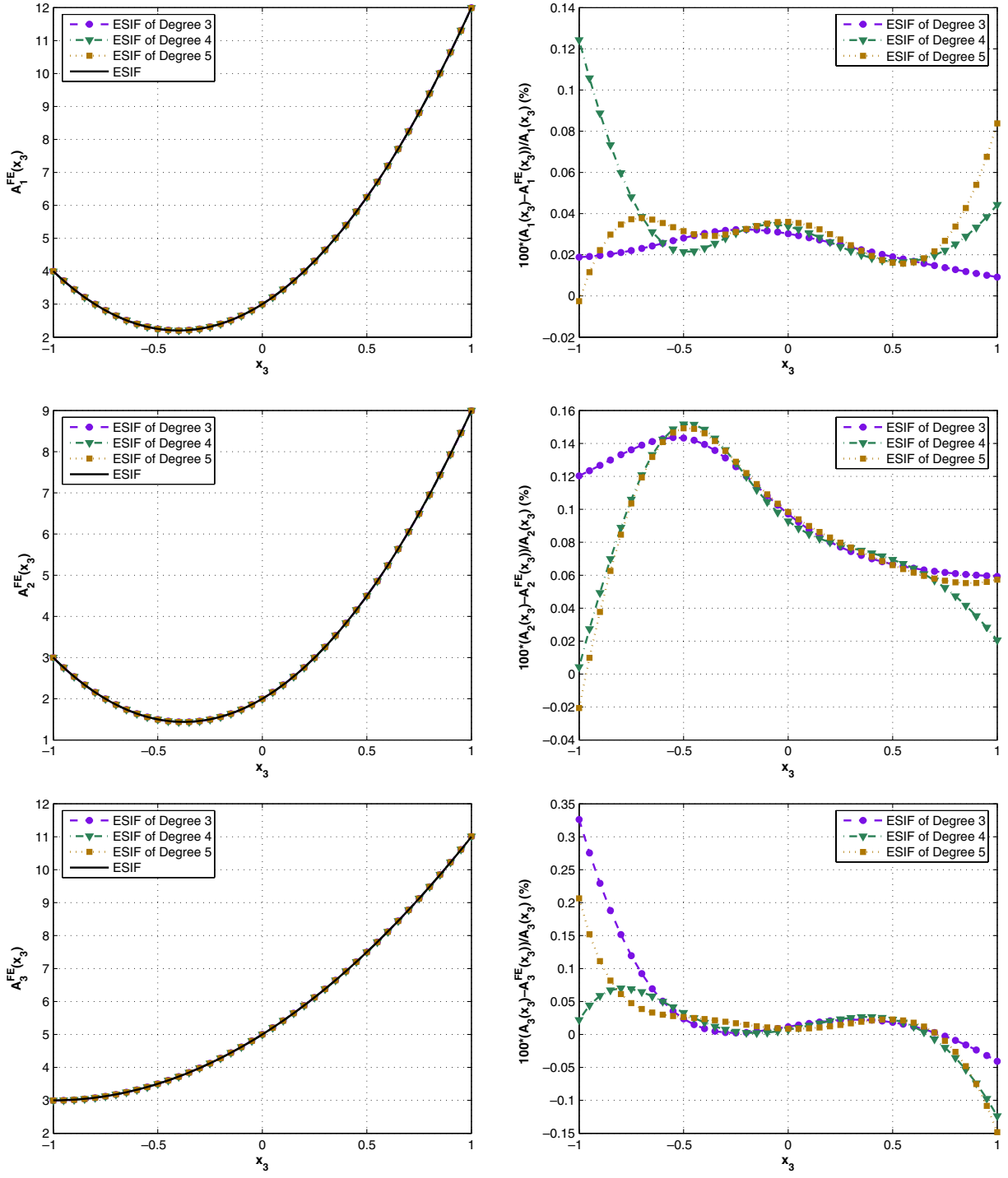

Fig. 14. ESIFs (left) and their relative error (right) extracted at $R = 0.05$ for anisotropic (82) cracked domain. Computations done with $B^{(k)}$, $k = 3, 4, 5$, where $A_1^{ex}(x_3) = 3 + 4x_3 + 5x_3^2$, $A_2^{ex}(x_3) = 2 + 3x_3 + 4x_3^2$, $A_3^{ex}(x_3) = 5 + 4x_3 + 2x_3^2$.

The relative error (as can be observed in Fig. 14) is lower than 0.5%. The results indicate that the eigen-functions, duals and shadows computed for the anisotropic domain are accurate and the ESIF extraction method performs well for anisotropic materials.

The results indicate that the solution in the vicinity of an edge for anisotropic domain may be computed numerically using the p-FEM method and the $J[R]$ integral, and obtain accurate and efficient results.

7. Summary and conclusions

The displacements in the vicinity of an edge for a 3-D elastic domain is described by a family of eigen-functions, shadow functions and their associated edge stress intensity functions.

In the case of anisotropic materials, there is no analytic solution to the eigen-pairs and shadows. Herein we presented a numerical method, based on the p-version of the finite element method for their computation. In isotropic domain the analytic solution is provided so the relative error of both primal eigen-functions and their shadows was shown to converge exponentially to less than 1%.

Next, the quasi-dual function method for ESIFs extraction was recalled. The implementation of the method was presented in [16] for scalar problems and in [22] for 3-D elastic isotropic problems. The results presented in this paper examine the accuracy of the method in the case of anisotropic domains for which the eigen-pairs, shadows and duals are computed numerically.

As a test case the ESIF was extracted for an isotropic domain for which the exact solution is known, using either analytical or numerical solution of the duals and their shadows. The results show that in both cases the relative error of the extracted ESIF was less than 1%. This indicates that the method is accurate and efficient.

Finally, ESIF extraction was performed for an anisotropic domain. Because the exact solution is unknown, the numerical computation of the eigen-pairs and shadows was considered instead. The relative error of the extracted ESIFs for the anisotropic problem was less than 0.5%.

The presented methods for the computation of eigen-pairs, shadow functions and the functional representation of ESIFs in the vicinity of edges are shown to apply to isotropic as well as anisotropic domains, are accurate and efficient. These methods are being extended to address problems having complex eigen-pairs and multi-material interfaces and will be reported in future publications.

Acknowledgements

The authors thank Profs. Monique Dauge and Martin Costabel of the UMR-CNRS 6625-IRMAR, Universite de Rennes 1, Campus de Beaulieu, Rennes, France, for helpful discussions, remarks and support.

Appendix A. Analytic solution of the eigen-pairs, duals and shadows for cracked domain ($\omega = 2\pi$) with traction free boundary conditions

For an isotropic domain with a crack ($\omega = 2\pi$) with traction free boundary conditions, the functions $\mathbf{\Phi}_0^{(\alpha_i)}, \mathbf{\Phi}_1^{(\alpha_i)}, \mathbf{\Phi}_2^{(\alpha_i)}$ and the dual functions $\mathbf{\Psi}_0^{(\alpha_i)}, \mathbf{\Psi}_1^{(\alpha_i)}$ and $\mathbf{\Psi}_2^{(\alpha_i)}$ may be computed analytically (see [22]).

$\mathbf{\Phi}_0^{(\alpha_1)}$ in the case of a crack is known as Mode I solution. The eigen-value in the case is $\alpha_1 = \frac{1}{2}$ and the primal and shadow functions for $\lambda = 0.5769$ and $\mu = 0.3846$ are

$$\mathbf{\Phi}_0^{(\alpha_1)}(r,\theta) = 0.084042 r^{\frac{1}{2}} \begin{pmatrix} 2.6\sin\left(\frac{1}{2}\theta\right) + \sin\left(\frac{3}{2}\theta\right) \\ 4.6\cos\left(\frac{1}{2}\theta\right) + \cos\left(\frac{3}{2}\theta\right) \\ 0 \end{pmatrix},$$

$$\mathbf{\Phi}_1^{(\alpha_1)}(r,\theta) = 0.084042 r^{\frac{3}{2}} \begin{pmatrix} 0 \\ 0 \\ -2\sin\left(\frac{1}{2}\theta\right) - 3.06667\sin\left(\frac{3}{2}\theta\right) \end{pmatrix},$$

$$\mathbf{\Phi}_2^{(\alpha_1)}(r,\theta) = 0.084042 r^{\frac{5}{2}} \begin{pmatrix} 0.23333\sin\left(\frac{1}{2}\theta\right) + 0.65644\sin\left(\frac{3}{2}\theta\right) \\ -0.76667\cos\left(\frac{1}{2}\theta\right) + 0.03244\cos\left(\frac{3}{2}\theta\right) \\ 0 \end{pmatrix}, \tag{A.1}$$

$$\boldsymbol{\Psi}_0^{(-\alpha_1)}(r,\theta) = 0.659433 r^{-\frac{1}{2}} \begin{pmatrix} \sin\left(\frac{1}{2}\theta\right) + 1.53333 \sin\left(\frac{3}{2}\theta\right) \\ \cos\left(\frac{1}{2}\theta\right) + 0.86667 \cos\left(\frac{3}{2}\theta\right) \\ 0 \end{pmatrix},$$

$$\boldsymbol{\Psi}_1^{(-\alpha_1)}(r,\theta) = 0.659433 r^{\frac{1}{2}} \begin{pmatrix} 0 \\ 0 \\ -1.73333 \sin\left(\frac{1}{2}\theta\right) - \frac{2}{3} \sin\left(\frac{3}{2}\theta\right) \end{pmatrix},$$

$$\boldsymbol{\Psi}_2^{(-\alpha_1)}(r,\theta) = 0.659433 r^{\frac{3}{2}} \begin{pmatrix} 0.23778 \sin\left(\frac{1}{2}\theta\right) - 0.1 \sin\left(\frac{3}{2}\theta\right) \\ 0.495556 \cos\left(\frac{1}{2}\theta\right) - 0.43333 \cos\left(\frac{3}{2}\theta\right) \\ 0 \end{pmatrix}. \tag{A.2}$$

Multiplying $\boldsymbol{\Phi}_0^{(\alpha_1)}(r,\theta)$, (A.1), by 0.32408, we obtain the classical Mode I solution. Comparing the 3-D solution presented herein with the 3-D test problem for Mode I presented by Meda et al. in [15] shows that both solutions are identical up to a constant.

$\boldsymbol{\Phi}_0^{(\alpha_2)}$ in the case of a crack is known as Mode II solution. The second eigen-value is $\alpha_2 = \frac{1}{2}$ and the primal and shadow functions ($\lambda = 0.5769, \mu = 0.3846$) are

$$\boldsymbol{\Phi}_0^{(\alpha_2)}(r,\theta) = 0.123947 r^{\frac{1}{2}} \begin{pmatrix} 0.86667 \cos\left(\frac{1}{2}\theta\right) + \cos\left(\frac{3}{2}\theta\right) \\ -1.53333 \sin\left(\frac{1}{2}\theta\right) - \sin\left(\frac{3}{2}\theta\right) \\ 0 \end{pmatrix},$$

$$\boldsymbol{\Phi}_1^{(\alpha_2)}(r,\theta) = 0.123947 r^{\frac{3}{2}} \begin{pmatrix} 0 \\ 0 \\ -0.66667 \cos\left(\frac{1}{2}\theta\right) \end{pmatrix},$$

$$\boldsymbol{\Phi}_2^{(\alpha_2)}(r,\theta) = 0.123947 r^{\frac{5}{2}} \begin{pmatrix} 0.07778 \cos\left(\frac{1}{2}\theta\right) - 0.07956 \cos\left(\frac{3}{2}\theta\right) \\ 0.25556 \sin\left(\frac{1}{2}\theta\right) + 0.10775 \sin\left(\frac{3}{2}\theta\right) \\ 0 \end{pmatrix}, \tag{A.3}$$

$$\boldsymbol{\Psi}_0^{(-\alpha_2)}(r,\theta) = 0.447126 r^{-\frac{1}{2}} \begin{pmatrix} \cos\left(\frac{1}{2}\theta\right) + 4.6 \cos\left(\frac{3}{2}\theta\right) \\ -\sin\left(\frac{1}{2}\theta\right) - 2.6 \sin\left(\frac{3}{2}\theta\right) \\ 0 \end{pmatrix},$$

$$\boldsymbol{\Psi}_1^{(-\alpha_2)}(r,\theta) = 0.447126 r^{\frac{1}{2}} \begin{pmatrix} 0 \\ 0 \\ -2 \cos\left(\frac{3}{2}\theta\right) \end{pmatrix},$$

$$\boldsymbol{\Psi}_2^{(-\alpha_2)}(r,\theta) = 0.447126 r^{\frac{3}{2}} \begin{pmatrix} -0.27067 \cos\left(\frac{1}{2}\theta\right) - 0.3 \cos\left(\frac{3}{2}\theta\right) \\ -0.31067 \sin\left(\frac{1}{2}\theta\right) + 1.3 \sin\left(\frac{3}{2}\theta\right) \\ 0 \end{pmatrix}. \tag{A.4}$$

Multiplying $\boldsymbol{\Phi}_0^{(\alpha_2)}(r,\theta)$, (A.3), by -0.17796, we obtain the classical Mode II solution for a crack.

$\boldsymbol{\Phi}_0^{(\alpha_3)}$ in the case of a crack is known as Mode III solution. The third eigen-value is $\alpha_3 = \frac{1}{2}$ and the primal and shadow functions ($\lambda = 0.5769, \mu = 0.3846$) are

$$\boldsymbol{\Phi}_0^{(\alpha_3)}(r,\theta) = 0.569394 r^{\frac{1}{2}} \begin{pmatrix} 0 \\ 0 \\ \cos\left(\frac{1}{2}\theta\right) \end{pmatrix},$$
$$\boldsymbol{\Phi}_1^{(\alpha_3)}(r,\theta) = 0.569394 r^{\frac{3}{2}} \begin{pmatrix} -0.29333\cos\left(\frac{1}{2}\theta\right) \\ 0.10667\sin\left(\frac{1}{2}\theta\right) \\ 0 \end{pmatrix},$$
$$\boldsymbol{\Phi}_2^{(\alpha_3)}(r,\theta) = 0.569394 r^{\frac{5}{2}} \begin{pmatrix} 0 \\ 0 \\ -0.3\cos\left(\frac{1}{2}\theta\right) \end{pmatrix}, \tag{A.5}$$
$$\boldsymbol{\Psi}_0^{(-\alpha_3)}(r,\theta) = 1.453475 r^{-\frac{1}{2}} \begin{pmatrix} 0 \\ 0 \\ \cos\left(\frac{1}{2}\theta\right) \end{pmatrix},$$
$$\boldsymbol{\Psi}_1^{(-\alpha_3)}(r,\theta) = 1.453475 r^{\frac{1}{2}} \begin{pmatrix} -0.13333\cos\left(\frac{1}{2}\theta\right) \\ -0.53333\sin\left(\frac{1}{2}\theta\right) \\ 0 \end{pmatrix},$$
$$\boldsymbol{\Psi}_2^{(-\alpha_3)}(r,\theta) = 1.453475 r^{\frac{3}{2}} \begin{pmatrix} 0 \\ 0 \\ -1.16667\cos\left(\frac{1}{2}\theta\right) \end{pmatrix}. \tag{A.6}$$

References

[1] T. Apel, V. Mehrmann, D. Watkins, Structured eigenvalue method for computation of corner singularities in 3D anisotropic elastic structures, Comput. Methods Appl. Mech. Engrg. 191 (2002) 4459–4473.
[2] A. Beagles, A.-M. Sändig, Singularities of rotationally symmetric solutions of boundary value problems for the Lamé equations, ZAMM – Z. Angew. Math. Mech. 71 (1991) 423–431.
[3] H. Blum, M. Dobrowolski, On finite element methods for elliptic equations on domains with corners, Computing 28 (1982) 53–63.
[4] M. Costabel, M. Dauge, General edge asymptotics of solution of second order elliptic boundary value problems I & II, Proc. Roy. Soc. Edinburgh 123A (1993) 109–184.
[5] M. Costabel, M. Dauge, Crack singularities for general elliptic systems, Math. Nach. 235 (2002) 29–49.
[6] M. Costabel, M. Dauge, Y. Lafranche, Fast semi-analytic computation of elastic edge singularities, Comput. Methods Appl. Mech. Engrg. 190 (2001) 2111–2134.
[7] M. Costabel, M. Dauge, Z. Yosibash, A quasidual function method for extracting edge stress intensity functions, SIAM J. Math. Anal. 35 (5) (2004) 1177–1202.
[8] M. Dauge, Elliptic Boundary Value Problems in Corner Domains – Smoothness and Asymptotics of Solutions, Lecture Notes in Mathematics, vol. 1341, Springer-Verlag, Heidelberg, 1988.
[9] P. Grisvard, Elliptic Problems in Nonsmooth Domains, Pitman Publishing, England, 1985.
[10] R.J. Hartranft, G.C. Sih, The use of eigenfunction expansions in the general solution of three-dimensional crack problems, J. Math. Mech. 19 (2) (1967) 123–138.
[11] O. Huber, J. Nickel, G. Kuhn, On the decomposition of the *J*-integral for 3D crack problems, Int. J. Fract. 64 (4) (1993) 339–348.
[12] S.N. Karp, F.C. Karal, The elastic field behavior in the neighborhood of a crack of arbitrary angle, Comm. Pure Appl. Math. 15 (1962) 413–421.
[13] D. Leguillon, E. Sanchez-Palencia, Computation of Singular Solutions in Elliptic Problems and Elasticity, John Wiley & Sons, New York, NY, 1987.
[14] V.G. Maz'ya, B.A. Plamenevskii, L^p estimates of solutions of elliptic boundary value problems in a domain with edges, Trans. Moscow Math. Soc. 1 (1980) 49–97.
[15] G. Meda, T.W. Messner, G.B. Sinclair, J.S. Solecki, Path-independent *H* integrals for three-dimensional fracture mechanics, Int. J. Fract. 94 (3) (1998) 217–234.
[16] N. Omer, Z. Yosibash, M. Costabel, M. Dauge, Edge flux intensity functions in polyhedral domains and their extraction by a quasidual function method, Int. J. Fract. 129 (2004) 97–130.
[17] J.R. Rice, A path independent integral and the approximate analysis of strain concentration by notches and cracks, J. Appl. Mech. 35 (2) (1968) 379–386.
[18] B.A. Szabó, I. Babuška, Computation of the amplitude of stress singular terms for cracks and reentrant corners, in: T.A. Cruse (Ed.), Fracture Mechanics: Nineteenth Symposium, ASTM STP 969, ASTM, Philadelphia, 1988, pp. 101–124.
[19] B.A. Szabó, I. Babuška, Finite Element Analysis, John Wiley & Sons, New York, 1991.
[20] B.A. Szabó, Z. Yosibash, Numerical analysis of singularities in two-dimensions. Part 2: Computation of the generalized flux/stress intensity factors, Int. J. Numer. Methods Engrg. 39 (3) (1996) 409–434.
[21] M.L. Williams, Stress singularities resulting from various boundary conditions in angular corners of plates in extension, ASME J. Appl. Mech. 19 (1952) 526–528.
[22] Z. Yosibash, N. Omer, M. Costabel, M. Dauge, Edge stress intensity functions in polyhedral domains and their extraction by a quasidual function method, Int. J. Fract. 136 (2005) 37–73.
[23] Z. Yosibash, B.A. Szabó, Numerical analysis of singularities in two-dimensions. Part 1: Computation of eigenpairs, Int. J. Numer. Methods Engrg. 38 (12) (1995) 2055–2082.